School of Physics

Trinity College Dublin
The University of Dublin

The Fast Transient Sky

Stage Transfer Report

Owen Johnson[†]
Radio Transients Group
March, 2024

Supervisor: Assoc. Prof. Evan Keane

[†]ojohnson@tcd.ie

Abstract

The Universe presents a dynamic canvas of transient objects where rapid changes can be observed over timescales from milliseconds to years. This report details the progress made to answer open questions about an array of objects in the transient sky. This includes the search for Pulsars, Fast Radio Bursts, technosignatures, Radio Stars, and Exoplanets. The amount of content on each topic is reflective of the amount of work carried out on each project to date with a breif abstract on each below.

Redback pulsars are a subclass of millisecond pulsars characterized by their intermittent radio emission and close binary systems with low-mass companions, typically white dwarfs or main sequence stars. These pulsars exhibit complex and varied behaviors, including state transitions, eclipses, and outbursts. Their study sheds light on the physics of compact binary evolution, mass transfer processes, and the formation of millisecond pulsars. Understanding redback pulsars provides insights into stellar astrophysics and the population of neutron stars in our Galaxy. To date their our are two dozen confirmed Redbacks systems. This report details on how to conduct radio searching and confirmation of redback candidates produced from the *Fermi* catalog.

The **Search for Extraterrestrial Intelligence** aims to find evidence of technosignatures, which can point toward the possible existence of technologically advanced extraterrestrial life. Radio signals similar to those engineered on Earth may be transmitted by other civilizations, motivating technosignature searches across the entire radio spectrum. In this endeavor, the low-frequency radio band has remained largely unexplored; with prior radio searches primarily above 1 GHz. This report discusses the methods and results of the first ever low frequency survey and the steps forward in progression the field of low frequency technosignature searches.

Detecting radio stars and exoplanets using LOFAR. The significance of radio emission as a probe into stellar and planetary plasma environments, particularly emphasizing the low-frequency range ($\leq$ 300 MHz) as a window into understanding phenomena such as Coronal Mass Ejections (CMEs) and auroral emissions. The project aims to ascertain the prevalence of radio emission from these celestial objects and explore the feasibility of detecting radio emission from exoplanets with LOFAR and the single Irish LOFAR station. The mechanism behind radio emission, notably is observed through CMEs in stars and auroral emissions in planets analogous to Jupiter. With the aim of better understanding radio emission phenomena in stellar and planetary systems, offering insights into their magnetic environments and dynamic processes.

Contents

Declaration

I hereby declare that this stage transfer report is entirely my own work and that it has not been submitted as an exercise for a degree at this or any other university.

I have read and I understand the plagiarism provisions in the General Regulations of the University Calendar for the current year, found at http://www.tcd.ie/calendar.

Signed: _____ Date: _____

Publications and Presentations

Publications

Johnson, O.A., Gajjar, V., Keane, E.F., et. al (2023). Simultaneous dual-site SETI with LOFAR international stations. Manuscript accepted for publication to AJ. arXiv:2310.15704

Presentations

1. Low Frequency's Place in SETI, January, 2024, PSETI Symposium, Penn State. [**Invited**]
2. Technosignatures with NenuFAR, December, 2023, Science at Low Frequencies IX, UvA.
   [**Accepted, Presented by Co-Author**]
3. SETI Science at 30 - 190 MHz, November, 2023, BLUK Workshop, SKAO.
   [**Invited**]
4. Technosignature Science at Low Frequencies, November, 2023, NASA Goddard Flight Center.
   [**Invited**]
5. Dual Site SETI Searches, 2023, International Astronautical Congress, Baku.
6. SETI using I-LOFAR, 2023, Irish Astonomy Meeting 49, University College Cork.

Physical Constants

Constant	Symbol	Value
Speed of Light	c	2.99792458×10^{8} m/s
Gravitational Constant	G	6.674×10^{-11} m^3 kg^{-1} s^{-2}
Planck's Constant	h	6.626×10^{-34} m^2 kg s^{-1}
Boltzmann Constant	k_B	1.381×10^{-23} m^2 kg s^{-2} K^{-1}
Stefan-Boltzmann Constant	σ	5.670×10^{-8} W m^{-2} K^{-4}
Electron Charge	e	1.602×10^{-19} C
Electron Mass	m_e	9.109×10^{-31} kg
Proton Mass	m_p	1.672×10^{-27} kg
Neutron Mass	m_n	1.675×10^{-27} kg
Solar Mass	$M_\odot$	1.989×10^{30} kg
Solar Radius	$R_\odot$	6.957×10^{8} m
Solar Luminosity	$L_\odot$	3.828×10^{26} W
Solar Temperature	$T_\odot$	5772 K
Jansky	Jy	10^{-26} W m^{-2} Hz^{-1}

1 A Prelude to Pulsars

When stars with a mass of at least $8\,M_\odot$ reach the end of their evolutionary stage they experience a depletion of nuclear fuel will and undergo a core collapse. This results in the star exploding as a supernova. Depending on the mass of the host star the Supernova will form a black Hole or a neutron Star. Based on the electron degeneracy pressure limit (Chandrasekhar, 1967, pp. 434 – 443) stars that fall in the range of 20 - 30 $M_\odot$ form neutron stars (Heger et al., 2003).

Neutron stars are supported against further collapse by the presence of neutron degeneracy pressure which arises from the Pauli exclusion principle. Strong nuclear forces between the neutrons also provides additional support against gravitational collapse. With these three opposing forces a stable equilibrium is formed (Shapiro and Teukolsky, 1983).

In turn, this makes neutron stars exceptionally dense, they are the densest known objects in the universe that emit light. The average density of a neutron star is 10^{17}kg/m^3 (Baym et al., 1971) and their radii are comparable to the size of cities, with radii of 10 - 20 km.

During collapse the conservation of magnetic flux plays a crucial role in the large strength magnetic fields that are observed in neutron stars along with contributions from the dynamo effect and frozen-in magnetic fields. The strength of a pulsar's magnetic field is on the order of 10^{12} - 10^{15} G (Michel, 1982).

Charged particles accelerate along the magnetic field lines in the magnetosphere of the neutron star. These particles emit electromagnetic radiation in a cone shape along the magnetic axis. If the magnetic axis is not aligned with the rotational axis of the neutron star, the radiation beam will sweep across the sky. This is known as a pulsar, a Galactic lighthouse.

1.1 The Population of Pulsars

At the time of writing, there are currently more than 3380 known pulsars. Since their discovery by Jocelyn Bell Burnell (Hewish et al., 1968), the population has grown immensely, but there remain many open questions about pulsar evolution and the subclasses that lie within the population as a whole. Similarly to how exoplanet populations are shown using the mass-radius diagram and stellar populations are shown using the Hertzsprung-Russell diagram, pulsar populations are shown using what is known as the $P - \dot{P}$ diagram.

P represents the pulsar's rotational period and $\dot{P}$ its derivative. These are key ways that pulsars are classified and studied in the context of their evolution. An example of a $P - \dot{P}$ diagram is shown in fig. 1.1. Different values on the plot indicate roughly the pulsar's age

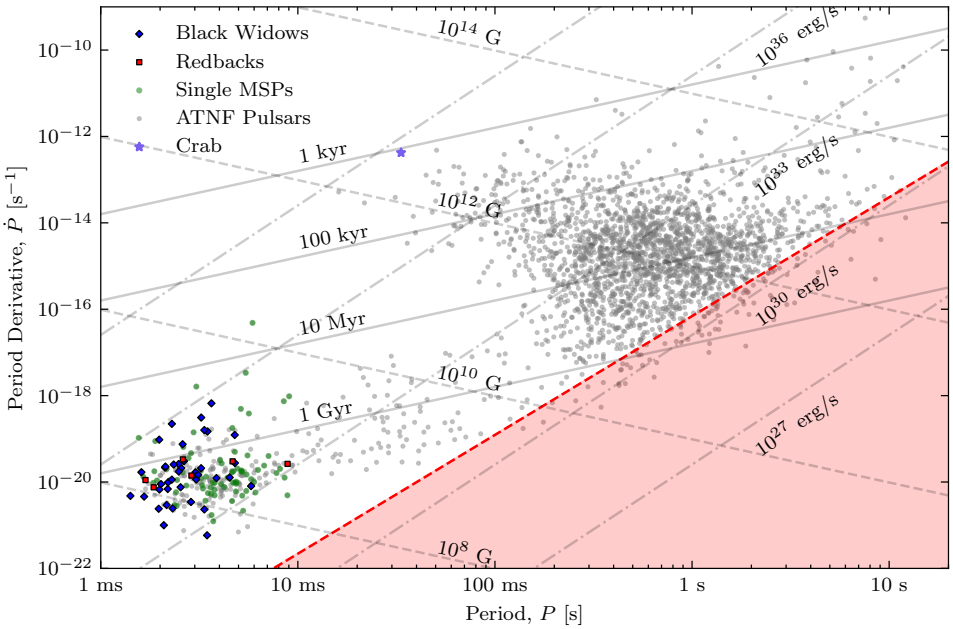

Figure 1.1: The $P - \dot{P}$ diagram showing the population of pulsars. The the millisecond pulsar subclasses are colour coded. The red region represents the death line, where pulsars are theoretically no longer able to emit radio waves.

and magnetic field strength. Figure 1.1 shows the vastly different values between pulsars in the millisecond range and pulsars in the second range.

Theoretically, it has been shown that pulsars can be related to a "death" line in the $P-\dot{P}$ diagram. This is the line where pulsars are no longer able to emit radio waves due to the pulsar's magnetic field no longer being strong enough to accelerate particles along the magnetic field lines. However, it has been shown that pulsars do exist below this line. The area below this line is commonly referred to as the "graveyard".

1.2 The Properties of Pulsars

The following section gives a brief non-exhaustive overview of some of the key properties of pulsars.

1.2.1 Neutron Star Radius & Mass

Understanding the mass of pulsars is important for understanding their evolution and equation of state. Oppenheimer and Volkoff (1939) derived a canonical mass limit of neutron stars to be 1.4 $M_\odot$, but experimentally, this has been shown to be higher, with the largest mass of a pulsar observed to be $\sim 2.35 M_\odot$ (Romani et al., 2022). The mass-radius relationship of a pulsar is defined by an equation of state and a maximum mass limit. Redshifts and gravitational effects observed in pulsars exhibit the observed temperature

and flux to be smaller than the actual value. The observed radius R_{obs} can be described as follows (p. 56 Lorimer and Kramer, 2004):

$$R_{\text{obs}} = \frac{R}{\sqrt{1 - \frac{2GM}{Rc^2}}} = \frac{R}{\sqrt{1 - \frac{R_s}{R}}} \tag{1.1}$$

where R is the pulsar's radius and M is the gravitational mass, G is the gravitational constant, c is the speed of light and R_s is the Schwarzschild radius. The lower limit of the neutron star radius is described by (p. 58 Lorimer and Kramer, 2004):

$$R_{\text{min}} \simeq 1.5\ R_s = \frac{3GM}{c^2} = 6.2\ \text{km}. \left(\frac{M}{1.4\,\text{M}_\odot}\right) \tag{1.2}$$

Opposite to this the upper limit of the radius is obtained by requiring that there is stability against breaking up due to centrifugal forces. This gives eq. (1.3) following as described in (Lorimer and Kramer, 2004, p. 58).

$$R_{\text{max}} \simeq \left(\frac{GMP^2}{4\pi^2}\right)^{1/3} = 16.8\ \text{km} \left(\frac{M}{1.4\,\text{M}_\odot}\right)^{1/3} \left(\frac{P}{\text{ms}}\right)^{2/3} \tag{1.3}$$

Most pulsars are theoretically thought to have radii in the range of 10 - 15 km (Lattimer and Prakash, 2001), giving them the unique position of 'almost' black holes.

1.2.2 Spin Evolution

One of the most unique characteristics of pulsars is the spinning that they exhibit. Understanding the spin evolution gives insight into many parameters of the pulsars, most notably the stage of their evolution. Pulsars begin their life in the upper end of the $P - \dot{P}$ diagram and slowly move down and to the right as they age due to a loss in rotational energy, commonly referred to as spin-down luminosity. The spin-down ($\dot{E}$) is described as follows (Lorimer and Kramer, 2004, p. 59):

$$\dot{E} = -\frac{dE_{\text{rot}}}{dt} = 4\pi^2 I \dot{P} P^{-3} \tag{1.4}$$

Where I is the moment of inertia. It is important to note that the energy loss that is converted into radio emission is almost negligible in comparison to the total energy loss from spin down.

1.2.3 Braking Index

Pulsars have strong magnetic dipoles. According to classical mechanics, a rotating magnetic dipole that exhibits a moment, $|m|$, emits an electromagnetic wave at the pulsar's rotation frequency (Lorimer and Kramer, 2004, p. 60). The dipole's radiation power is characterized by:

$$\dot{E}_{\text{dipole}} = \frac{2}{3c^3}|m|^2\omega^4 \sin^2\alpha \tag{1.5}$$

Where α is the angle between the magnetic axis and the rotation axis. Equating the above equation to the loss of rotational energy described in eq. (1.4) gives the following for the expected evolution of the period:

$$\dot{\Omega} = -\frac{2}{3Ic^3}|m|^2\Omega^3 \sin^2\alpha \tag{1.6}$$

This is more commonly written as a power law,

$$\dot{\nu} = -K\nu^n \tag{1.7}$$

Equation (1.7) in terms of the period is $\dot{P} = KP^{2-n}$. Since this is a first-order differential equation, the solution can be integrated and given a constant, K, which provides an expression of age:

$$T = \frac{P}{(n-1)\dot{P}}\left\{1 - \left(\frac{P_0}{P}\right)^{n-1}\right\} \tag{1.8}$$

Here P_0 is the initial period of the pulsar. Commonly an assumption is made that the current period is much greater than the initial period ($P_0 \ll P$). If it is also assumed that the pulsar is spinning down to due dipole magnetic radiation ($n = 3$), eq. (1.8) can be simplified into a characteristic age.

$$\tau_c \cong 15.8 \text{ Myr}\left(\frac{P}{s}\right)\left(\frac{\dot{P}}{10^{-15}}\right)^{-1} \tag{1.9}$$

The above estimation for a pulsars age is known to be inconsistent with theory to varying degrees. In cases where a Supernovae has been observed and has produced a pulsar the age is known to a much higher degree of accuracy. The Crab pulsar is one such example with an observed Supernova event in 1054 AD by Chinese astronomers (Kaspi et al., 2001).

1.2.4 Dispersion Measure

The interstellar medium (ISM) is a complex mixture of gas, dust and magnetic fields that fills the space between stars in a galaxy. Given that the ISM is a cold and ionised plasma any electromagnetic radiation will undergo a frequency-dependant index of refraction as they propagate. The following equation describes the refractive index of the ISM neglecting Galactic magnetic field (Lorimer and Kramer, 2004, p. 85),

$$\mu = \sqrt{1 - \left(\frac{f_p}{f}\right)^2} \tag{1.10}$$

Where f_p is the plasma frequency, 8.5 kHz $(n_e/\mathrm{cm}^{-3})^{1/2}$ and f is the frequency of the observed radiation.
If the refractive index of the ISM $\mu < 1$ then it can be assumed that the group velocity of the radiation is $v_g = c\mu$ which is sub light speed. The path of radiation from a pulsar to the observer will be delayed in time with respect to an infinite frequency by an amount:

$$t = \left(\int_0^d \frac{dl}{v_g}\right) - \frac{d}{c} \tag{1.11}$$

If is assumed to be $f_p \ll f$, μ can be approximated.

$$t = \frac{1}{c}\int_0^d \left(1 + \frac{f_p^2}{2f^2}\right) dl - \frac{d}{c} = \frac{e^2}{2\pi m_e c}\frac{\int_0^d n_e \, dl}{f^2} \equiv \mathcal{D} \cdot \frac{\mathrm{DM}}{f^2} \tag{1.12}$$

Where $\mathcal{D}$ is the dispersion constant and DM is the dispersion measure. Each are commonly expressed as follows, $\mathcal{D} = 4.15 \times 10^3$ MHz^2 pc^{-1} cm^3 s and DM $= \int_0^d n_e \, dl$ cm^{-3} pc. This definition was adapted from Lorimer and Kramer (2004, p. 86) and Taylor and Manchester (1977).

1.3 Spider Pulsars

One type of pulsar that is of interest to this project is a subclass of transitional millisecond pulsars known as spider pulsars. Spider pulsars fall into two categories depending on their orbiting companion. The first category are known as Black Widow pulsars, segregated based on their companion mass falling in the range of 0.01 - 0.05 $\mathrm{M}_\odot$ with a companion orbital period (P_B) of less than 10 hours. The second category are known as Redback pulsars and have a companion mass of 0.2 $\mathrm{M}_\odot$ or greater with a P_B of less than 1 day (Papitto and de Martino, 2022).

It is thought that most millisecond pulsars are formed through the accretion of matter

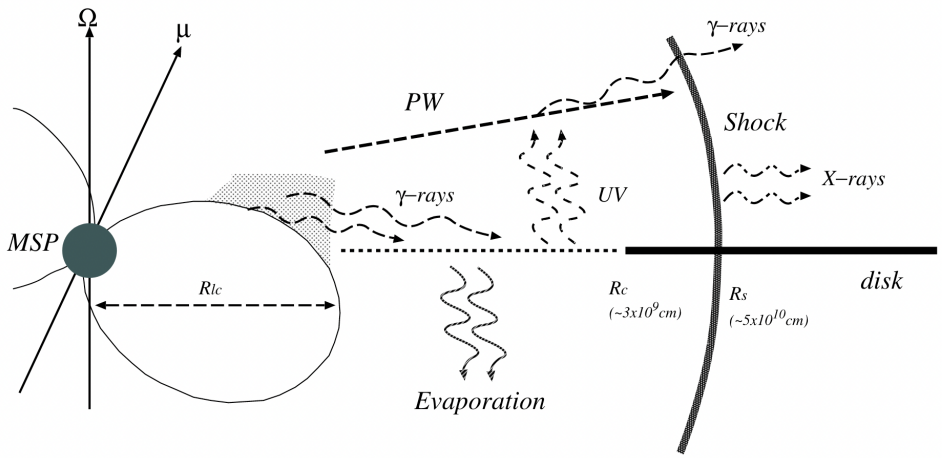

Figure 1.2: Figure taken from Takata et al. (2014). Example of multiwavelength emission from a Redback pulsar.

from an evolved compact binary system; the approximately 30% found in isolation are thought to have ablated their companion star to the point of disassociation (Strader et al., 2019). Material being thrown off the pulsar causes the radio emission to be eclipsed via scattering and absorption, for a segment of the companion's orbit. Redback systems exhibit both positive and negative period derivatives that are larger than the expected gravitational radiation and are thought to arise from the interaction of the companion's magnetic field and the pulsar's wind (Papitto and de Martino, 2022).

Redback pulsars have been observed in two transitional states: ablation and accretion states (Papitto and de Martino, 2022). These states are on sub-year timescales. The transition in stages sees the magnitude of optical emission increase by about one order of magnitude. Studying optical emission from redback pulsars informs on the heating of the companion, Roche-lobe filling fraction, and the mass of the system (Archibald et al., 2009; Roberts et al., 2017). Black widow pulsars have been observed to have little to no observable X-ray emission (Roberts et al., 2017). However, redbacks have been shown to exhibit much more X-ray emission in their thermal spectra with consistent double peaks observable when the pulsar is at inferior conjunction (Roberts et al., 2017). The observed companions of redbacks are mostly faint stars with temperatures around 2000 K on the farside of the star from the pulsar (Breton et al., 2013). The companion's interaction with the pulsar dominates the thermal spectrum of spider pulsars from the present heating between the two. X-ray emission from redbacks shows hard X-ray spectra that follow a power law with photon indices (Γ) around 1 - 1.3. The energy of the thermal spectra in the X-ray is higher than what is expected from shock acceleration. Some models suggest a wind-wind shock between the pulsar and companion. However, this approach would require the wind momentum of the pulsar to be much weaker than the companion's. Similarly with the optical emission, the X-ray emission may be influenced by the magnetic

field of the companion (Papitto and de Martino, 2022).

Redback's have also been known to emit γ-rays and is often the means in which Redback candidates are found. The primary source of gamma-ray emission in pulsar binaries is the pulsed magnetospheric radiation from the pulsar itself. Apart from a distinct dip observed in the light curves of eclipsing systems (Clark et al., 2023; Corbet et al., 2022), it has been traditionally believed that gamma-ray emission remains consistent throughout the orbital cycle.

1.4 Why study Redback Pulsars?

Redback pulsars have a number of interesting science cases. Redbacks undergo a range of phenomena, including radio and X-ray pulsations, accretion processes, and periodic eclipses as the companion star passes in front of the pulsar. Their study also provides valuable insights into the evolution of binary systems, the behavior of pulsars, and the physics of accretion processes. Due to their transitional nature, they provide a glimpse into the evolution of pulsars in the latter stages of their life cycle. Pulsars are also used as tools to study theories of gravity, the interstellar medium, and probe for gravitational waves.

1.5 Other exotic transients

Redbacks themselves are exotic transients, but there are many other classes of radio exotic that are of interest to the community. In this project, work has also been carried out on an array of various radio transients and related objects. This includes the search for extraterrestrial intelligence (SETI), the study of M and Brown dwarf radio flares, and the probing of potential radio emission from exoplanets.

1.5.1 Radio Stars and Exoplanets

It has been well documented that our own star, the Sun, and planets in the solar system have radio emission associated with originating from auroras and stellar flares (Murphy et al., 2021; Zarka, 1998). With the advancement of modern radio telescopes, the prospect for capturing radio emission from others and even the prospect of detecting an exoplanet magnetosphere has become achievable (Vedantham et al., 2020).

Observing stars especially at low frequency ($\leq$ 300 MHz)[1] act as probes into stellar and planetary plasma environments. Coronal Mass Ejections (CMEs) have a low-frequency burst component in which information about the kinematics of plasma can be deduced

[1] $\lambda \sim 1$ m

(Villadsen and Hallinan, 2019). Incident solar wind is also the primary driving force of auroral emission on magnetized planets. The goal of this project is to explore the viability of detecting radio emission from M and Brown dwarfs using I-LOFAR observations and archive data to put constraints on the prevalence of radio emission from these objects and explore the viability observing radio emission from exoplanets.

Radio emission from stars is typically produced through CMEs, observed phenomenologically in the Sun as type II and III solar bursts. The radio emission from these events is thought to be produced through the electron-cyclotron maser instability (ECMI; Zheleznyakov and Zlotnik, 1975). The ECMI is a plasma instability that occurs in the presence of a magnetic field and a population of energetic electrons. The instability is thought to be the primary driver of radio emission observed in type II bursts and stars as a whole. With type III bursts being thought to be the result of electron beams that are accelerated in the corona.

Emission from planets has also been observed in the form of auroral emission. The most notable example of this is the Jovian system. The Jovian system is known to have auroral emission that is driven by the interaction of the solar wind with the magnetosphere of the planet. Coherent radio emission from the aurora is thought to be produced through the cyclotron maser instability (ECM; Zarka, 1998) which injects a high-velocity electron population into the magnetosphere. The maximum frequency of the ECM is directly proportional to the magnetic field strength of the object at its emitting point (Kavanagh and Vedantham, 2023; Callingham et al., 2024).

Much time has been spent observing Ultracool Dwarfs (M7 <) as they provide a good analogue to the Jovian systems. This allows for direct comparison between the two. This provides valuable insights into the formation, atmospheric processes, and potential habitability of gas giants like Jupiter. Moreover, such comparative studies contribute significantly to our understanding of planetary evolution and diversity beyond our immediate neighbourhood. Recent detection of radiation belts around a UCD further supports the analogy to Jupiter, as radiation belts are a key characteristic of Jupiter's magnetosphere (Callingham et al., 2024). UCDs, being intermediate in mass between stars and planets, serve as a bridge to understanding exoplanet detection. The discovery of bursting radio emission from a brown dwarf and subsequent detections in UCDs indicate departures from established stellar coronal/flaring relationships. Radio bursts from UCDs can exhibit periodic timing (Hallinan et al., 2006) along with strong circular polarization and high brightness temperatures, suggesting the involvement of the ECM process in generating radio emission. Despite a significant amount of gigahertz-frequency radio searches, detection rates for UCD radio emissions remain stubbornly low at around 10% overall (Lynch et al., 2016).

1.5.2 The Search for Extraterrestrial Intelligence

The search for life elsewhere in the Universe has always been a burning question for many astronomers throughout history. Moreover, the prevalence of intelligent life in the universe has been a particularly intriguing aspect of this quest. Since the 1960s, astronomers have conducted consistent surveys, mainly in radio, aimed at detecting signals of artificial origin, commonly referred to as "technosignatures". These signatures are thought to resemble radio signals produced artificially on Earth and are mainly hypothesized to be narrowband drifting radio emissions leaking into space from transmitters. However, to date, there has been no positive detection of a technosignature.

Similar to searches for dark matter, the lack of detection's has allowed researchers to place limits on the prevalence of civilizations in the galaxy. During the first radio Search for Extraterrestrial Intelligence (SETI) survey, Drake (1961) coined an equation to estimate the prevalence of civilizations in the local galaxy.

$$N = R_* \cdot f_p \cdot n_e \cdot f_l \cdot f_i \cdot f_c \cdot L \tag{1.13}$$

Where N is the number of civilizations in the galaxy, R_* is the rate of star formation, f_p is the fraction of stars that have planets, n_e is the number of planets that could potentially support life, f_l is the fraction of planets that develop life, f_i is the fraction of planets that develop intelligent life, f_c is the fraction of planets that develop technology, and L is the lifetime of the civilization. However, in this endeavour there has been little to no SETI conducted at low frequencies in the radio regime as illustrated in fig. 1.3. The main science goals of a low frequency technosignature search is to place tight constraints on the Drake equation at these frequencies, study methods on RFI mitigation and also use the high resolution data collected to search and study other radio transients, such as magnetars, Fast Radio Bursts (FRBs), pulsars and M-dwarfs.

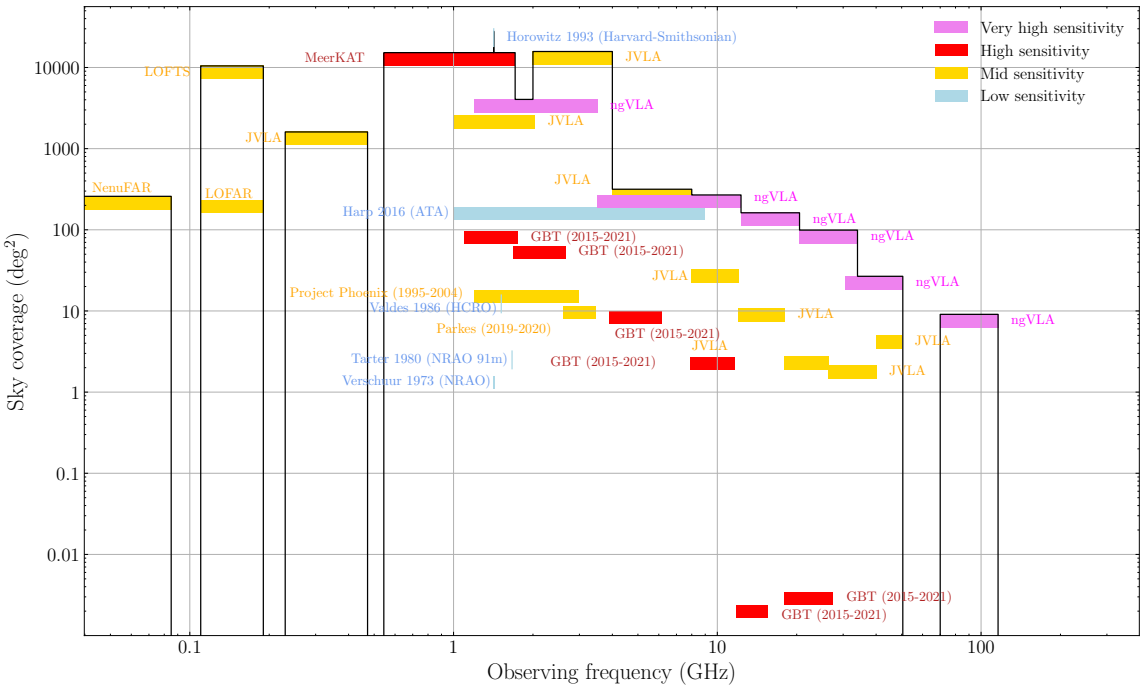

Figure 1.3: The radio frequency parameter space covered by technosignature searches as a function of sky coverage and sensitivity. The color coding represents the ability to detect an Arecibo-like planetary transmitter at various distances. Where $d_* \leq 25$ pc, $d_* \leq 75$ pc and $d_* \leq 250$ pc are shown in blue, green and red respectively. With anything beyond 250 pc being shown in pink. The figure is adapted from Ng et al. (2022).

2 Pulsar Searching in a Binary System

As outlined in section 1 the study of redback pulsars has a multitude of science cases. However, the number of known redback is small, in searching for new redback pulsars allows for further inquiry into the nature of the subclass. The search usually begins with the selection of potential candidates from large-scale surveys carried out by optical, X-ray and γ-ray observatories. Candidates are determined based on the flaring exhibited at these shorter wavelengths, then followed up using radio telescopes. Work to date has been to perform follow-up radio observations of Redback candidates to attempt to confirm radio emission and further compliment prior multi-wavelength studies.

The *Fermi* Large Area Telescope (LAT) provides the most candidates as the related γ-ray emission are not subject to the same limitations as other detection methods (Ray et al., 2012). Both candidates observed so far as part of this project are two *Fermi* candidates 1FGL J0523.5-2529 and 4FGL J2054.2+6904.

2.1 Observation Campaigns

J0523 was the first observed candidate and was observed using the Ultra-Wide-Bandwidth, Low Frequency Receiver (UWL)[2] on the Parkes Murriyang telescope in New South Wales. Published studies from Strader et al. (2014) and Halpern et al. (2022) provide the orbital period, companion's radial velocity and distance measurements for the system. Each of these factors are important in determining the observation and search strategy.

For the pulsar to be detected the radio emission from the poles must be visible to the observer plane of view and the beam must not be obscured by the companion star. The orbital phase can be easily calculated from the periodic emission in the optical as demonstrated in fig. 2.1 using the following equation,

$$\phi = \frac{t - T_0}{P_{\text{orb}}} \tag{2.1}$$

At the time of writing 74% of the orbital phase has been observed, with time approved to observe the remaining orbital phase if the pulsar is not detected.

In the case of J2054 less information is known with no accurate phase ephermeris available. A study by Karpova et al. (2023) reports the period, companion radius and distance. Over 8 hours of observations have been carried out using I-LOFAR. In this case the entire orbit needs to be covered and blindly searched for radio emission within expected parameter range of a Redback pulsar. Observations with OSMOS, the Ohio State Multi-Object Spectrograph (Martini et al., 2011) are planned to take place in the Summer of 2024 to try and determine the time of ascending orbital phase.

2.2 Observation Data

Observations from radio telescopes typically includes measurements of intensity, frequency, polarization and time. The data is usually stored in a time series format with the intensity and frequency measurements recorded at each time step. The data is usually stored in a filterbanks (`.fil`) or .fits file format. The raw voltages are recorded and then processed into usable Stoke I files.

2.3 Search Strategy

A zoo of pulsar software has been developed over the past decades to detect and time pulsars. One of the most commonly used software in the search for binary pulsars is

[2]The UWL operates from 704 to 4032 MHz (40 - 7 cm)

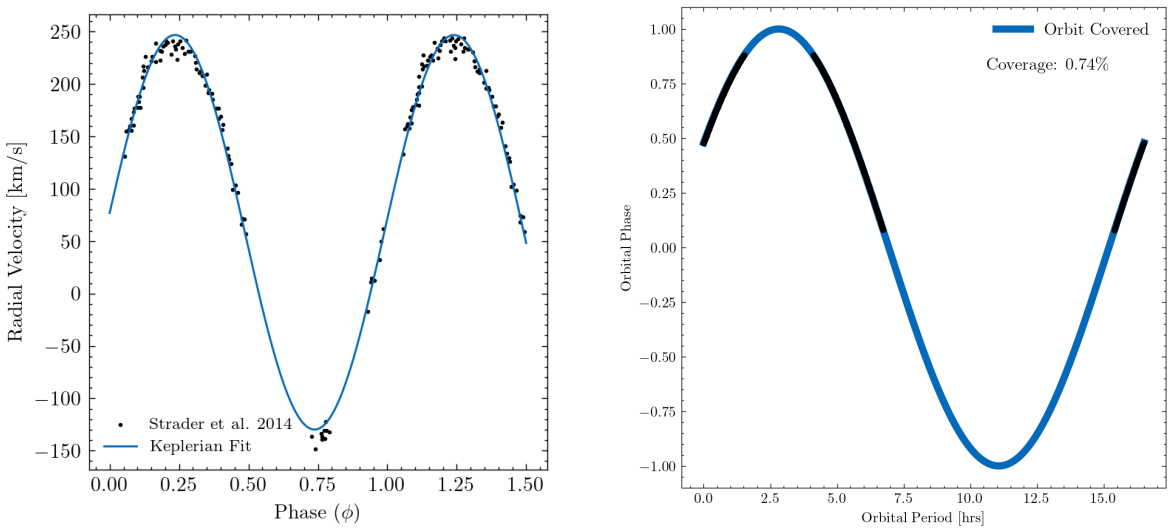

(a) **(b)**

Figure 2.1: *(a)* Phased radial velocities observed from the optical counterpart of J0523 with the Keplerian fit plotted on top. *(b)* Observed orbital phase of J0523 with Parkes UWL to date.

PRESTO (Ransom, 2001). The search is carried out as illustrated in fig. 2.2 and due to the large data volumes produced by modern telescopes, the search is carried out in a distributed manner on high performance computing clusters.

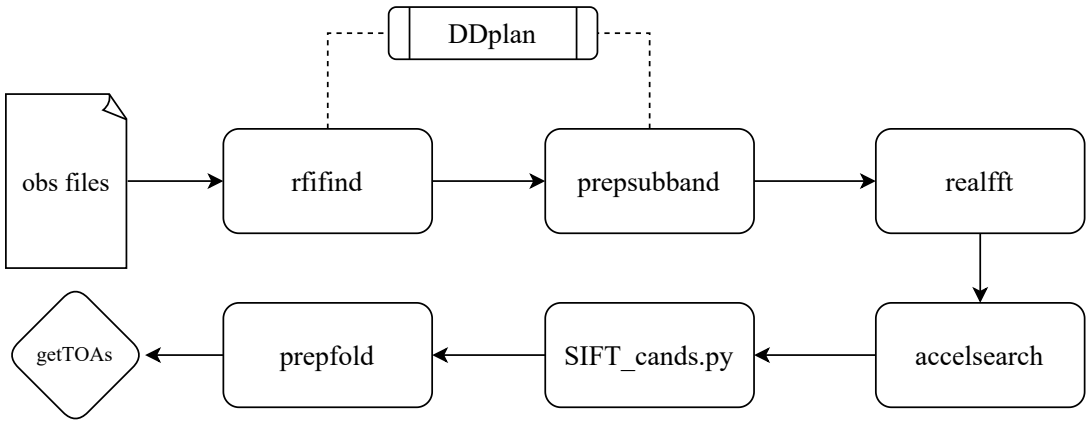

Figure 2.2: Outline of the PRESTO search strategy used to search for binary pulsars.

2.3.1 RFI Removal

The first step in nearly all radio observations is to remove Radio Frequency Interference (RFI) from the observations data, this is usually caused by most modern technologies. This is important as artifical signals can mimic period signals associated with pulsar emission. Thus the data must mask frequencies or be clipped in the time domain. This project makes use of `rfifind` to remove such RFI.

`rfifind` which is part of the PRESTO suite searches in both frequency and time domains.

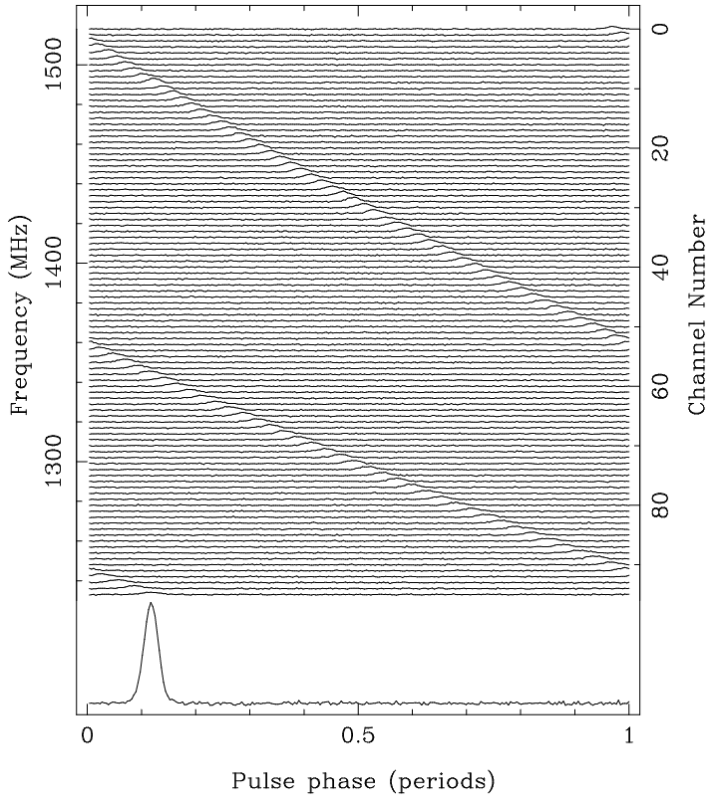

Figure 2.3: Example of a dispersion pulses of 128 ms pulsar B1356-60, which has a dispersion measure of 295 pc cm^{-3}. Figure from Lorimer and Kramer (2004, p. 20).

It analyses each channel for a specified time integration. Firstly the time domain statitics are computed which consists of the mean and standard deviation of the values in each channel. For blocks where the mean value exceeds 4σ the block is flagged as RFI. If more than 30% of the channel is flagged the entire channel is masked completely and replaced with a median constant band-pass value. An example of a mask produced by `rfifind` is shown in fig. 2.4.

2.3.2 Incoherent Dedispersion

Following the masking of all observation files the next step is to incoherently dedisperse the data. This is done to remove the effects of dispersion caused by the interstellar medium as discussed in section 1.2.4. Failure to de-disperse data broadens potential pulse profiles and significantly reduces the signal to noise ratio. Figure 2.3 shows an example of pulse dispersion. Incoherent dedispersion is carried out by splitting the data into sub-bands and then shifting the data in time to correct for the dedispersion.

When correcting for dispersion it is important to consider the possible range of DMs that the pulsar could exhibit. The DM can be estimated through the use of density electron models such as Cordes and Lazio (2003) and Yao et al. (2017). However when dedisperseing the data it inherently induces smearing in the data. There are four types

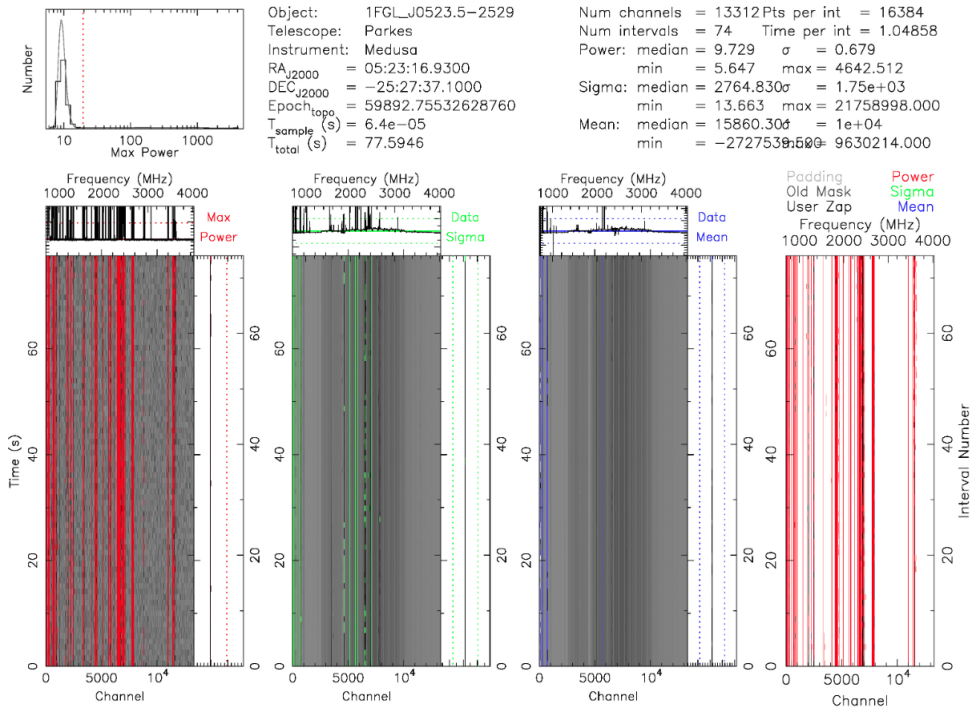

Figure 2.4: Example of RFI removal using `rfifind` on a 77 second observation of J0523. The upper left panels shows the max power profile of the RFI detected. The bottom most left panel show the max power, the second panel to the right shows the σ, the third panel shows the mean and the right most panel is the recommended mask with all panels plotted.

of smearing that need to be accounted for and characterized by the following equation,

$$\tau_{\text{total}} = \sqrt{\tau_{\text{samp}}^2 + \tau_{\text{sub}}^2 + \tau_{\text{BW}}^2 + \tau_{\text{chan}}^2} \tag{2.2}$$

Where τ_{chan} is the channel smearing, τ_{samp} is the sample time, $\tau_{\text{sub}}$is the subband smearing and τ_{BW} is the bandwidth smearing. Coherent dedispersion entails mitigating dispersion effects by employing the complex conjugate of the interstellar medium's transfer function to deconvolve the data before undergoing filterbanking. By adopting this approach, the original instrumental or Nyquist time resolution is preserved, ensuring high sensitivity and minimal smearing, thereby facilitating the detection of millisecond pulsars (Hankins and Rickett, 1975).

2.3.3 Fast Fourier Transform

The data is needs to be transformed into the frequency domain to search for periodic signals. This is commonly done with a Discrete Fourier Transform (DFT) in pulsar astronomy and computationally carried out using a Fast Fourier Transform (FFT). For a time series, S_j of a given length of N it is necessary to convert the time series into the barycentric frame of reference. The barycentric frame if reference point is centered on the mass of the solar system.

The kth Fourier component of the time series is described in Lorimer and Kramer (2004, pp. 132–134) as,

$$\mathcal{F}_k = \sum_{j=0}^{N-1} S_j \exp\left(-2\pi\sqrt{-1}\frac{jk}{N}\right) \tag{2.3}$$

To complete this computation it requires N^2 floating point operations. However, if a FFT operation is employed the number of operations is reduced to $N \log_2 N$ for a time series of length N. Since the time series data are real numbers symmetry can be exploited as the DFT is symmetric about the Nyquist frequency, $\nu_{\rm Nyq} = 1/(2t_{\rm samp})$. For any frequencies higher than the $\nu_{\rm Nyq}$ the complex conjucate is the same as the corresponding lower half of the frequency.

On the software side this is carried out with the `realfft` function in PRESTO. This result intakes the dedisperesed sub-bands and returns the power spectrum of the data. At this point the data is in a state to be searched for periodic signals.

2.3.4 Accelration Searching

Searching for binary pulsars requires a slightly different approach as the motion of the system causes the observed pulse frequency to smear across the Fourier bins (Ng et al., 2015), in turn this reduces the sensitivity of the search. A solution to this is to split up the search into smaller time intervals and assume that the radial velocity is a constant on this time scale. This can be shown to be a good approximation for $P_b/10$.
The spin frequency, $f_{\rm spin}$ and the time of pulse emission, $t_{\rm pulse}$ the pulsar's phase can be expressed as, $\phi_p = f_{\rm spin} t_{\rm pulse}$. Moreover, the pulse time can be expressed as the time of arrival from the pulsar, $d(t_0)$,

$$t_{\rm pulse} = t_0 - \frac{d(t_0)}{c} \tag{2.4}$$

thus the phase can be expressed as,

$$\phi_p = f_{\rm spin}\left[t_0 - \frac{d(t_0)}{c}\right] \tag{2.5}$$

$$= f_{\rm spin}\left[t_0 - \frac{a\sin i}{c}\sin\left[\frac{2\pi(t - t_{\rm asc})}{P_B}\right]\right] \tag{2.6}$$

where a is the semi-major axis, i is the inclination angle, $t_{\rm asc}$ is the time of ascending node and P_B is the orbital period. A Taylor expansion can be used to $\sin x$ around $x = a$ such that,

$$\sin(x) \simeq \sin(a) + \cos(a)(x-a) - \frac{\sin(a)}{2!}(x-a)^2 - \frac{\cos(a)}{3!}(x-a)^3 + \dots \tag{2.7}$$

Therefore the phase of the pulsar with a constant spin down rate can be expressed as,

$$\phi(t) = f^1 t_0 + \frac{\dot{f}}{2}(t-t_0)^2 + \frac{\ddot{f}}{6}(t-t_0)^3 + \dots \tag{2.8}$$

Matching co-effcients between the the full Taylor expansion and the phase expression for the pulsar gives the following relation, $\dot{f}/2 = f_{\text{spin}} \frac{a \sin i}{c} A$. Where A is represents all the terms in the expansion. The final simplified expression works out to be,

$$\dot{f} = f_{\text{spin}} \frac{4\pi^2 a \sin i}{c P_B^2} \sin\left[\frac{2\pi(t - t_{\text{asc}})}{P_B}\right] \tag{2.9}$$

Thus over a small enough time period spin-down is approximately constant.

$$\frac{k_2 P_B}{2\pi q} = a \sin i \tag{2.10}$$

Where k_2 is the radial velocity semi-amplitude, P_B is the orbital period and q is the mass ratio.

Searching is carried out using `accelsearch` which searches the FFT time series for period emissions by summing the highest Fourier frequency derivative. The number of bins that this signal is smeared is given by the acceleration parameter (Ransom, 2001),

$$z \simeq \dot{f} T_{\text{obs}}^2 \tag{2.11}$$

Where T_{obs} is the length of the observation. The search is carried out over a range of accelerations which can be based on eq. (2.10) if the physical quantities are known. A list of the known orbital parameters for the two candidates is given in table 1 along with resultant z values.

Candidate	P_{orb} (days)	k_2 (kms^{-1})	$a \sin i$ (s)	e	q	z
J0523.5-2529	0.68813	190.3	0.359	0.040	0.61 ± 0.06	$3.56 - 335.36$
J2054	0.31111	...	...	...	...	...

Table 1: Orbital parameters of the two candidates. Values for J0523 are taken from Strader et al. (2014) and Halpern et al. (2022). Values for J2054 are taken from Karpova et al. (2023).

In cases where the orbital parameters are not known the search is carried out over a range of accelerations from 0 to 200, and even in the case where the value exceeds 200, this is left as a cap on the search. The reason that the search is not carried out over the entire

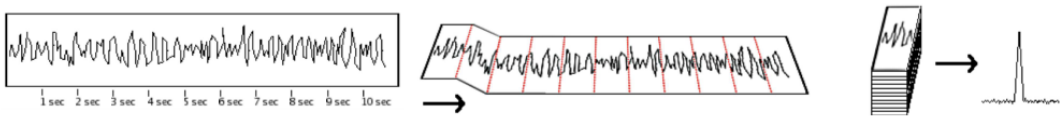

Figure 2.5: Adapted illustration from Kumar and Western (2021) of the folding process. The left panel shows the observed time series, the middle panel shows the folded time series and the right panel shows the summed pulse profile.

range is due to the computational cost and is often not necessary with accelerations above 200 starting to exhibit a non-linear relationship as stated in Ransom (2001). Once the search is carried out the results are outputted in the form of candidates with estimates on DM, S/N, period and frequencies.

2.3.5 Folding

Pulsar folding is a technique commonly used when the pulses are not bright enough to be clearly visible in the observed time series. The term folding comes from the fact that the time series is folded on itself by some trial period of the pulsar, this is illustrated in fig. 2.5.

Using a routine called `prepfold` each of the candidates over the noise floor are folded with each candidate examined by eye for possible positive pulsar detection. An example of this is shown in fig. 2.6. This plot contains integrated pulse profile, time series plot and sub-band plot. It also shows DM, P and $\dot{P}$ plots as a function of reduced χ^2 values. Each of these plots must be sifted through by eye. A pulsar will exhibit a single high S/N peak in the DM, P and $\dot{P}$ plots similar to those shown in the plot if its a positive candidate.

3 Technosignature Searches at Low Frequencies

The first year of the project primarily entailed the publication (Johnson et al., 2023) of results from the first search for technosignatues at low frequency using Irish and Swedish LOw Frequency ARay (I-LOFAR; van Haarlem et al., 2013). When carrying out this technosignature search the two main goals were to constrain the prevalance of intelligent civilizations in the Milky Way at an unexplored frequency and use the collected data to search for other exotic transients such as Fast Radio Bursts (FRBs), pulsars, magnetospheres and M-dwarf emission (Sheikh, 2020). The following sections will detail the means and methods on how technosignature search is carried out.

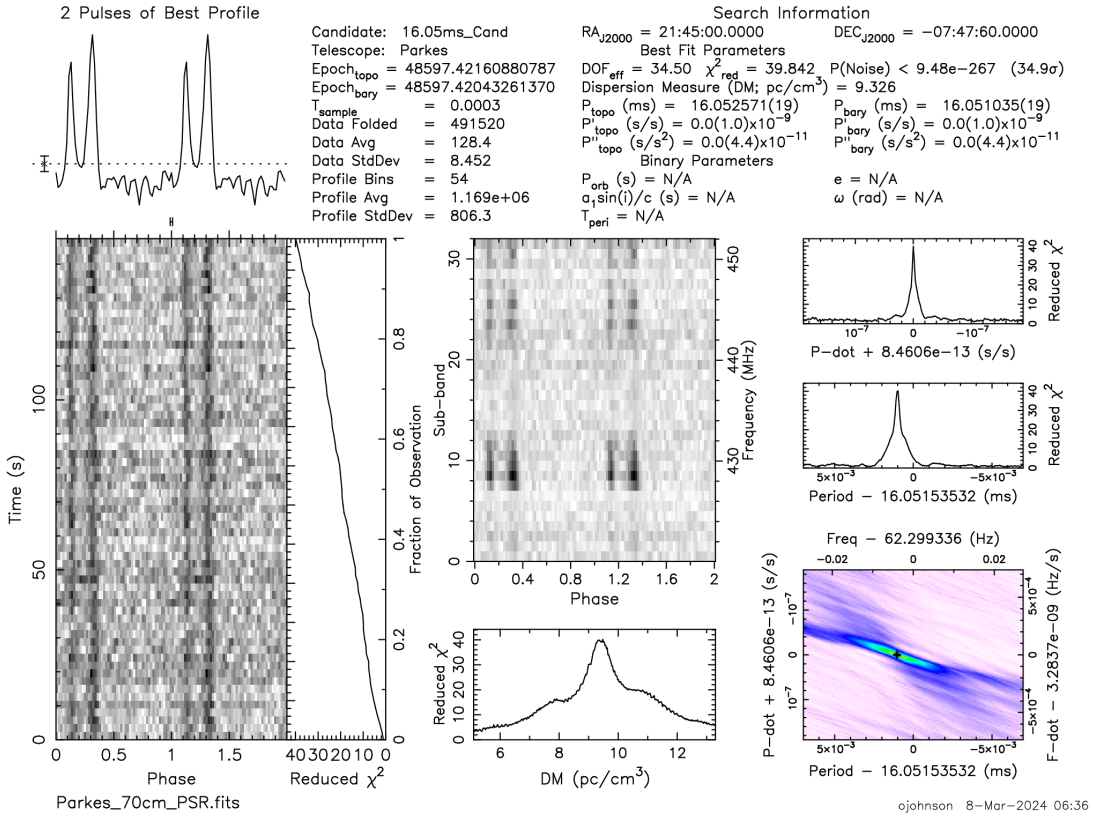

Figure 2.6: Example of a `prepfold` plot for J2145-0750 using described pipeline.

3.1 LOFAR

LOFAR, a pioneering low-frequency aperture array telescope, spans hundreds of kilometers across Europe and serves as a pathfinder to the Square Kilometer Array (SKA). The array consists of a core station with outrigger stations situated in the Netherlands and additional international stations spanning multiple countries, such as Germany, France, Sweden, Ireland, Latvia, Poland, and the United Kingdom. Additionally, stations are currently in the process of being constructed in Italy and Bulgaria. The LOFAR array operates using two types of antenna, the Low Band Antenna (LBA) and the High Band Antenna (HBA), operating at 10–90 MHz and 100–250 MHz respectively[3]. In this study, the HBAs at the Irish and Swedish LOFAR station are used to carry out observations non interferometrically. The field of view (FoV) of an international LOFAR station is rather large; at full width at half maximum, it is 5.3, 3.4, and 2.3 deg^2 at frequencies of 120, 150, and 180 MHz, respectively (van Haarlem et al., 2013). The station is capable of resolution of 3.3 and 0.2 arcsecond at the bottom and the top of the bad respectively when the entire array is in use making it one of the most sensitive telescopes in the world.

[3]LBA: $\lambda \sim 30 - 3$ m; HBA: $\lambda \sim 3 - 1$ m

3.2 Target Selection

A significant fraction of radio emission from Earth is emitted in the direction of the ecliptic plane. For example, powerful planetary radars are used to explore Solar System objects (Siemion et al., 2013), and high-powered transmitters are used to communicate with Solar System probes (Enriquez et al., 2017). It is conceivable then that such leakage radiation may also be emanating from other worlds, preferentially in their planetary orbital planes. This is why we chose TESS targets, as these are the closest transiting exoplanet systems known (Borucki et al., 2010; Ricker et al., 2015). Observing these sources with the LOFAR HBAs enables robust constraints on any associated artificial low-frequency radio emission

3.3 Expanding the Cosmic Haystack

Searching for technosignatures is akin to searching for a needle is a cosmic sized haystack thus it is important to extend area of the haystack as much as possible. The beam of a LOFAR station has an expansive coverage enabling observation of a substantial number of stars in the field of view. The significance of these in-field stars has been highlighted by Wlodarczyk-Sroka et al. (2020). Consequently, during our observations targeting 44 sources from the TESS catalog, we encountered a significant number of in-field stars within our field of view. To determine the list of targets within this field of view, the *Gaia* catalog is utilized. Some previous major SETI surveys focused their searches toward Sun-like stars (Tarter, 1996). However, because our understanding of the origin of life is limited, it makes sense to allow for the possibility of life arising on a planet that is neither Earth-like nor around stars that are Sun-like. Similarly, planets not necessarily located in the habitable zone should be considered. This is typically characterized as the orbital range wherein liquid water could exist (Kasting et al., 1993), as inferred from planetary equilibrium temperatures often ignoring the unknown albedo of the exoplanets. Any sensitive radio SETI survey seeking to maximize the chance of detecting weak radio signals should, insofar as possible, expand its search to encompass nearby stars of a broad range of spectral types and with exoplanets of all sizes and distances from their parent star. Thus, calculations were conducted to determine the number of Gaia stars with a mean distance of 1215 pc, with an accuracy in their distances of at least 20%. This study used Gaia's third data release (GDR3; Gaia Collaboration et al., 2023; Ginsburg et al., 2019). When analyzing GDR3, two filters were applied to the survey volume and sensitivity accuracy of the in-beam target values. First, a constraint on the R.A. and decl. errors was implemented. If a Gaia source was found to be in the beam but had an error magnitude greater than the FWHM, it was removed from the source pool. Equation (3.1) states the first condition of filtering:

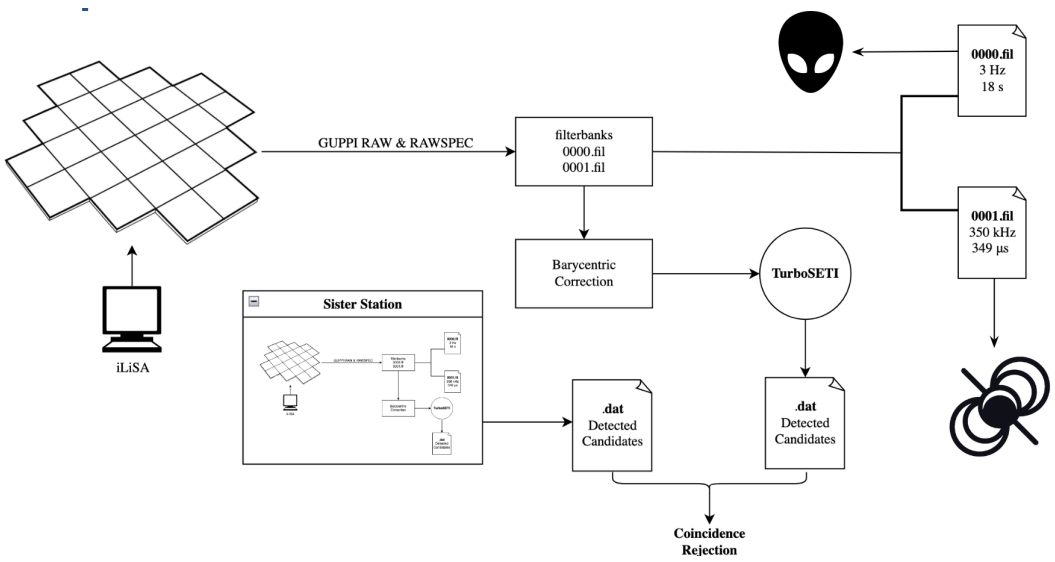

Figure 3.1: Outline of the SETI pipeline developed and deployed on Breakthrough Listen nodes at both LOFAR stations.

$$\theta_{\text{sep}} + \sqrt{\Delta\text{RA}^2 + \Delta\text{Dec}^2} \leq \frac{\text{FWHM}}{2} \tag{3.1}$$

As the sensitivity of the survey is calculated based on a source's distance, a second filter is implemented to remove sources that have large errors. By taking the difference ($\Delta\sigma_G$) in the upper and lower confidence levels of GSP-Photometry, we obtain a percentage error on distance. All sources with a d_{M_G} error of 20% or greater are filtered out of the source list. Equation (3.2) states the second condition of filtering:

$$\frac{\Delta\sigma_G}{\sigma_G} \leq 20\% \tag{3.2}$$

A total of 1,631,152 stars form this list, making it one of the largest samples of stars ever surveyed for SETI purposes.

3.4 Carrying out a Dual-Site Survey

Typically, international LOFAR stations operate as standalone telescopes $2-3$ days per week, i.e. they do not operate as part of the International LOFAR Telescope's Europe-wide array. This project was undertaken during this standalone time. For this purpose the *international LOFAR in Stand-Alone mode* (`iLiSA`) package[4] is used to control both telescopes simultaneously. `iLiSA` provides a high-level operational control of multiple LOFAR stations, including scheduling, processing pipeline dispatching and metadata aggregation. For the observations in this study, an operator-produced list of targets that

[4] https://github.com/2baOrNot2ba/iLiSA/releases/tag/v6.1

were close[5] to the local meridian was fed into `iLiSA` at each epoch. Towards each target, one beam per station was formed using `iLiSA`, and each beam was formed with 412 HBA sub-bands (corresponding to a bandwidth of 80.46875 MHz). The scan time on each target was 15 min, and the whole scheduling block was a few hours per epoch. Data was preproccessed[6] and prepared using the `udpPacketManager` package (McKenna et al., 2023). Which resulted in two sets of filterbanks for each observation, each with different frequency and time resolutions. The first set of filterbanks had a frequency resolution of 2.98 Hz and a temporal resolution of 0.67 s. The second set of filterbanks had a frequency resolution of 350 kHz and a temporal resolution of 349 µs. The first set of filterbanks was used for the search for narrowband technosignatures, and the second set was used for the search for broadband transients. A broad overview of the pipeline employed is shown in fig. 3.1.

3.5 Narrowband Search Results

Using `turboSETI`, a Doppler-drift search was carried out on the observed candidates at both stations. This resulted in the list of "hits" collected, where hits are defined as a narrowband signal detected above the given threshold, S/N = 10. The distribution of narrowband signals detected at both stations is shown in fig. 3.2. A large percentage of hits are seen at both sites in the 120-140 MHz range. This falls within the range of expected RFI leakage seen from neighboring airports[7]. Using a drift-rate search of ±4 Hz/s for this study covers a fraction of the possible drift rates of transmitters from exotic objects that can be detected as outlined by Sheikh et al. (2019). Li et al. (2022) shows that 4 Hz/s is comprehensive in relative to the expected distribution of exoplanet drift rates. The omission of a search outside this parameter space is due to its computationally intense nature of searching for narrow-band signals across a sizeable drift-rate range. However, in doing this, the parameter space searched for extra terrestrial intelligent (ETI) signal has been drastically reduced. Continual development of search algorithms like `turboSETI` is progressing to make larger drift-rates searches a more computationally feasible. Upon first inspection of Figure 3.2 it appears that the results at both stations are somewhat similar. However, upon performing a Kolmogorov-Smirnov (KS) test for each set of results for drift-rate, SN and frequency of detected hits the highest p-value returned was on the order of 10^{-11} indicating that the RFI environments at each of the stations are significantly different. In the case of this study, a singular beam observes a single target for 15 minutes at both stations and observations are converted to barycentric reference frame. Narrow-band searches are then performed at both sites, and the results of both

[5] In practice as Birr and Onsala are separated by ~ 20 deg of longitude, the optimum scheduling is to observe ~ 40 min$-T_{\rm obs}/2$ 'late' at Onsala and 40 min$+T_{\rm obs}/2$ 'early' at Birr.

[6] For detailed explanation of the preprocessing and preperation see Lebofsky et al. (2019)

[7] Shannon & Goteborg Landvetter.

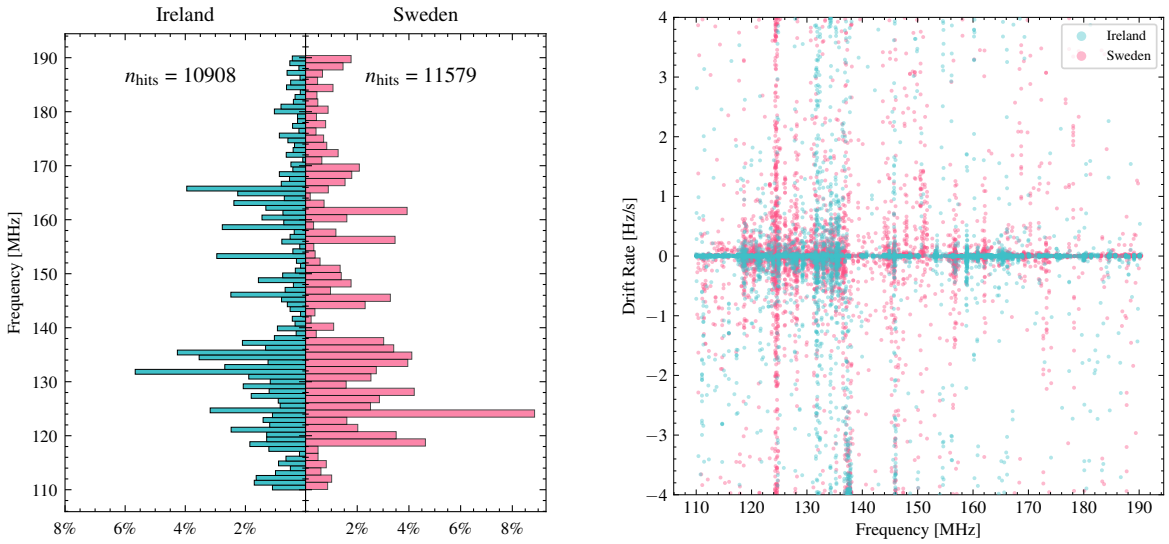

Figure 3.2: *(a)* Comparison of drifting signals or "hits" detected at both stations seen across the HBA frequency band. Each bin within the data set represents a 1 MHz frequency range and is accompanied by a corresponding percentage indicating its proportion to the overall data set. *(b)* A scatter plot of the drift-rate values against detected frequency. The Irish station is shown in pink and the Swedish station is shown in blue.

searches are compared.

In our analysis, a signal is classified as a mutual extraterrestrial hit only if two conditions are met: *a)* the signals are within a frequency range of ±4 Hz of each other in the barycentric reference frame, and *b)* their drift rates are within ±0.2 Hz/s of each other after barycentric drift corrections. In the topocentric frame, a detected narrowband signal at 160 MHz that is simultaneously present at both stations. However, when converting to the barycentric reference frame, the signal appears to be seen at different frequencies with opposite signs due to the different line-of-sight velocities towards the target with both signals differing by 300 kHz. As a result, this narrowband signal is rejected as a genuine sky-bound signal.

3.6 Constraints placed by the Survey

Even though the survey resulted in the non-detection of a narrowband signal it is important to place constraints on the probed parameter space. The required power for a certain (ETI) transmitter to be detected depends on its directionality and other signal characteristics. The transmitter power of an ETI beacon can be measured in terms of the effective isotropic radiated power (EIRP; Enriquez et al. 2017) as,

$$\text{EIRP} = \sigma \times 4\pi d_\star^2 \frac{\text{SEFD}}{\delta\nu_t}\sqrt{\frac{\delta\nu}{n_p t_{obs}}}\ \text{W} \tag{3.3}$$

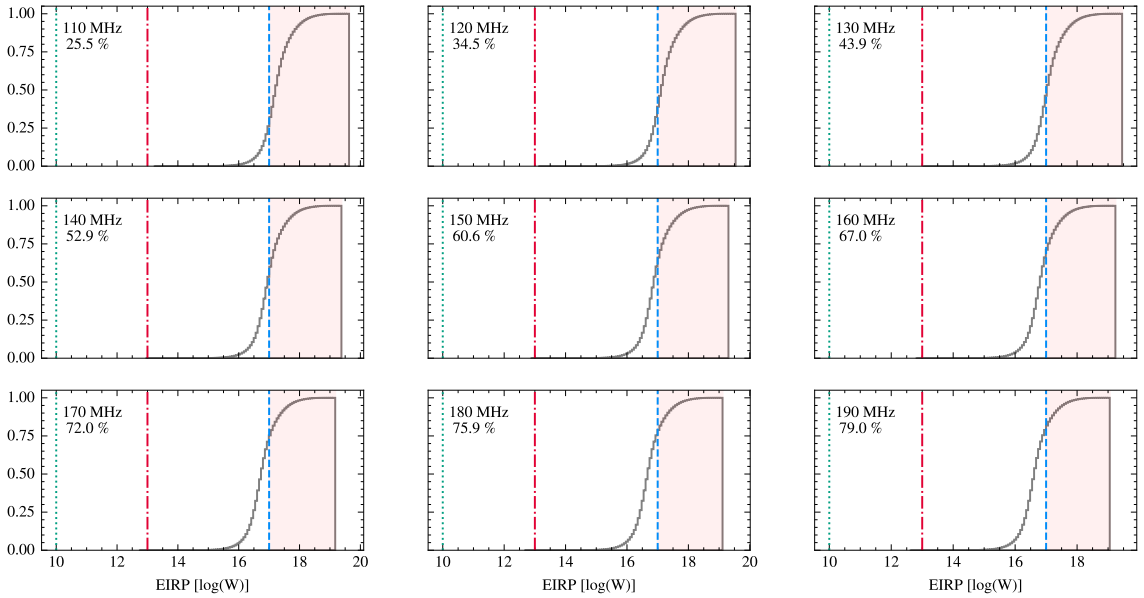

Figure 3.3: Cumulative histogram of EIRP limits of this survey across the HBA band. Reference luminosities for three civilization Kardeshev levels emitting 10^{17},10^{13} or 10^{10} W are shown in blue, red, and green respectively. The percentage of targets where the station is sensitive to the transmission of 10^{17} W is shown, as a function of frequency across the band. At lower frequencies, sensitivity to 10^{17} emitters drops off as the $T_{\rm sys}$ rises. The $\bar{T}_{\rm sys}$ varies from 1260 K down to 322 K as frequency is increased across the band. Detailed calculations are presented in Appendix B of Johnson et al. (2023).

Here, σ is the required S/N, $\delta\nu$ is the bandwidth of the received signal, $\delta\nu_t$ is the transmitted bandwidth, t_{obs} is the observing integration time, SEFD is the System Equivalent Flux Density, n_p is the number of polarizations, and $d_\star$ is the distance between the transmitter and the receiver, i.e., the distance to the star. We considered $\delta\nu_t$ to be 1 Hz. For the narrowband signals we consider in our Doppler searches, we assume $\delta\nu$ is matched to our spectral resolution and further assume a temporal duty cycle of 100%. Figure 3.3 presents the luminosity limits for the cumulative targets of this survey within the frequency range of $110 - 190$ MHz. In this figure, the limiting luminosity is compared to notable values of Equivalent Isotropic Radiated Power (EIRP) for various scenarios. These scenarios include a Kardashev I type advanced civilization transmitting at a power level of 10^{17} W, an advanced civilization producing planetary radar-level transmissions with a transmitting power of 10^{13} W, and a cumulative aircraft radar-type system transmitted across a large solid angle with a power of 10^{10} W (Siemion et al., 2013). The figure demonstrates that due to the varying system temperature (T_{sys}) across the frequency band, our observations were sensitive to detecting a range of Kardashev I type targets. Specifically, we were able to detect approximately 25% of the targets at the lower end of the frequency band, increasing to nearly 80% of the targets at the higher end of the band.

A modified variation of the Drake equation (Eqn. 3.4; Shklovskii and Sagan 1966; Gajjar et al. 2022) is used to constrain the fraction of narrowband emitting civilizations (f_c^n).

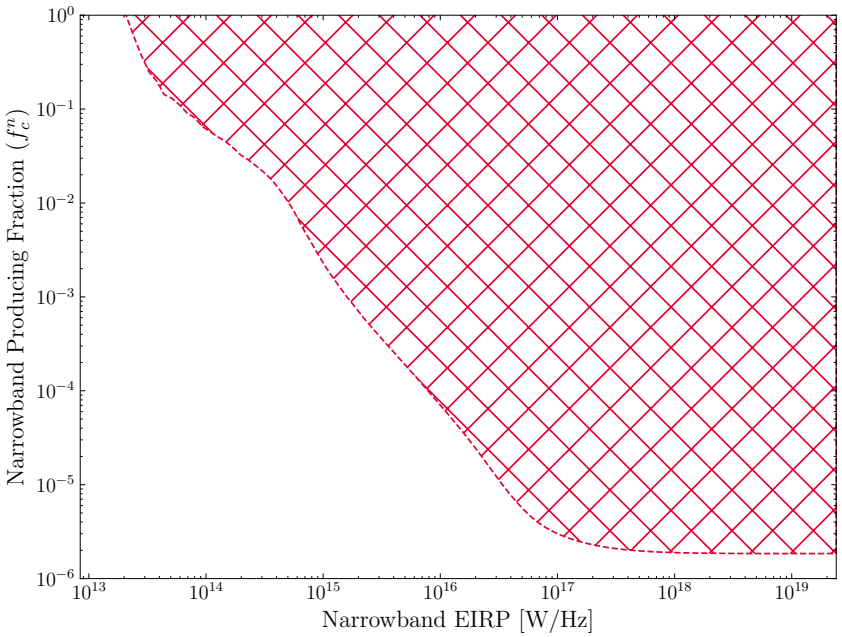

Figure 3.4: The fraction of stars that produce narrow-band emission (f_c^n) against the transmitter power of the total target pool. The hashed region (red) shows the constraints this survey places on a value of f_c^n at 110 - 190 MHz.

$$N = R_{\mathrm{IP}} f_c^n L \tag{3.4}$$

Here R_{IP} is defined as the emergence rate (yr^{-1}) of intelligent life in the Milky Way. Figure 3.4 shows the constraint that this survey places on f_c^n when using a Poisson sided upper limit at 95% confidence which in this case is 2.995 as per Gehrels (1986). This provides the most stringent constraint of f_c^n in this frequency range.

LOFAR is soon to undergo a staged series of upgrades across all stations in the array. These upgrades at individual stations across Europe will involve the installation of a new Receiver Control Unit (RCU) as described in ASTRON (2023). These RCUs will enable the simultaneous use of both the LBA and HBA in the frequency range of 15 - 240 MHz. This enhancement will allow for a SETI survey across a broader low-frequency band. Specifically, at 30 MHz, the FWHM will cover an area of 19.39 deg^2, decreasing to 1.73 deg^2 at 190 MHz. This will enable follow-up LOFAR surveys to encompass a larger volume of stars and a broader frequency domain. Additionally during the roll out of the 2.0 upgrade the international stations will be switched into local mode for months at a time. This gives ample opportunity to carry out additional observation campaigns to form the basis of a LOw Frequency pulsar, FRB, and Technosignature Survey (LOFTS). LOFTS will entail a persistent zenith pointings to sweep out sections of the northern hemisphere with a larger t_{obs} and lower T_{sys}, greatly improving both the volume and sensitivity of its prior survey.

4 Forward Plan

As of writing this there has been a single publication from this project (outlined in section 3) with numerous other in preparation for publication. Figure 4.1 outlines the estimated timeline for the completion of all outlined projects. A brief overview of the projects at their status is outline below in order of expected completion date.

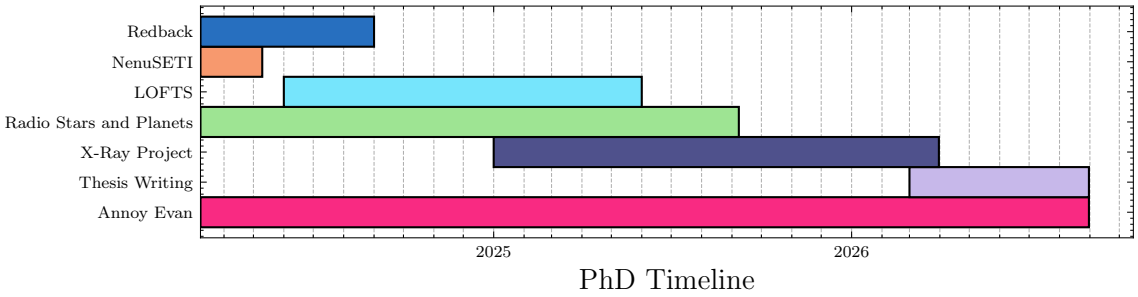

Figure 4.1: Estimated timeline for completion of projects that will make up overall PhD. Each increment on the grid is equivalent to 1 month. With the start time marked as March 8th 2024.

4.1 NenuSETI

This project utilized the New Extension Upgrading LOFAR (NenuFAR) based in Nançay. NenuFAR is the most sensitive standalone low-frequency telescope in the Northern Hemisphere, operating at 10 - 95 MHz. Over the past number of observation cycles, a significant number of observations have been taken. These observations have targeted exoplanets confirmed by Kepler and more recently TESS. Baseband data will be collected for a subset of the TESS catalog in the low frequency band (clean of RFI), reduced into high time and frequency resolution Stokes-I data products at 1.49 Hz and 671 ms resolution, and then finally searched for drifting narrowband signals. As SETI is a key program on NenuFAR, it directly aims to assist other science cases in radio astronomy.

Axis 1: A dedicated TESS exoplanet and targets of interest (TOI) follow-up program, where baseband data will be collected for a subset of the TESS catalog in the 39.8-67.7 MHz band (clean of RFI), reduced into high time and frequency resolution Stokes-I data products at 1.49 Hz and 671 ms resolution, and then finally searched for drifting narrowband signals.

Axis 2: Commensal search associated with the “Exoplanets & Stars” and “Cosmic Dawn” Key Programs, searching high-resolution data products (of the order of 1 Hz resolution) for artificial emissions originating from distant stellar systems and the Northern Celestial Pole. Moreover, this project will also periodically conduct a high-resolution survey of the RFI environment of NenuFAR and develop an interface for RFI data visualization and analysis.

The first axis of the NenuSETI project has had 80% of the analysis completed. This paper is currently being drafted and once some system administration with the BL back-end in Nançay is complete, the paper will be swiftly submitted no later than the end of April 2024. Preliminary constraints set on technosignatures in this frequency range can be seen in fig. 4.2.

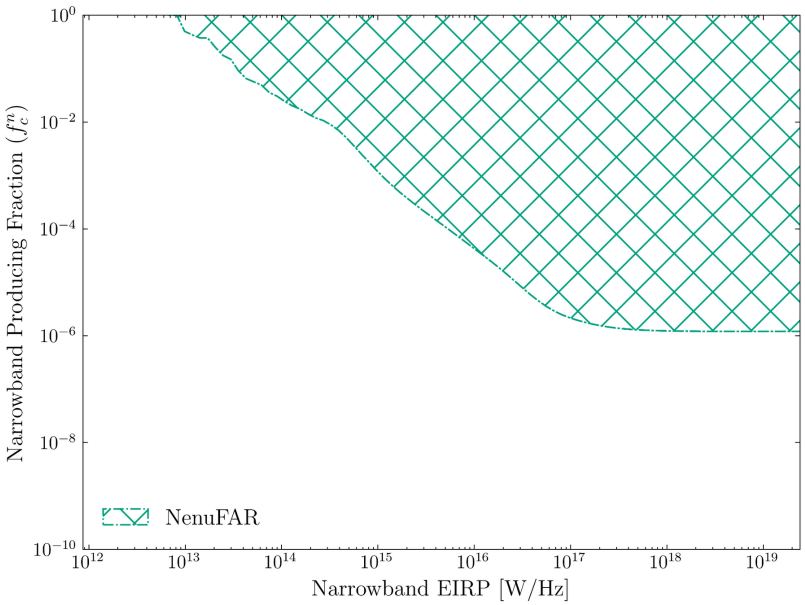

Figure 4.2: The preliminary fraction of stars that produce narrow-band emission (f_c^n) against the transmitter power of the total target pool. The hashed region (red) shows the constraints this survey places on a value of f_c^n at 30 - 95 MHz.

4.2 Redback Pulsar Searches

The redback pulsar search employs full analysis pipelines, as detailed in section 2, which are written and deployed on the OzStar supercomputing cluster at Swinburne University and the REALTA back-end in Birr. At present, all data from J2059 has been processed, with expanded trials underway in an attempt to detect the pulsar. Processing of data from J2054 is currently at 50% completion but has been temporarily halted due to bottlenecks in the back-end system. We anticipate publishing either a pulsar detection or non-detection by the end of August 2024.

4.3 Low-Frequency FRB, Pulsar and Technosignature Search

As previously discussed in section 3, the observation campaign is expected to commence following the roll-out of LOFAR 2.0 upgrades to the core stations in the Netherlands. This is anticipated to occur in the early summer months of 2024. Consequently, all remote

stations will be allocated 100% of observing time, allowing for the accommodation of the large amount of observation time required for LOFTS.

Automated pipelines for handling the data have been written and tested on operational backends. The deployment of the BL backend to the Chilboltan station is expected to be completed in the coming months, upgrading the survey's status to tri-site. Methods will be carried out in a similar manner as described in section 3.

4.4 Radio Stars and Exoplanets

To date, the project has conducted 13 hours of bright M-dwarf observations on two radio bright sources: CR Draconis and TVLM 513-46. The primary objective is to establish a pipeline capable of reliably identifying radio emissions from these sources. Following this, the focus will shift to observing fainter sources, specifically brown dwarfs and planetary systems exhibiting signs of emission resulting from exoplanetary-stellar interactions.

Observations are taking place on a weekly basis of bright M dwarfs and being actively processed into 8 bit filterbanks in each of the Stoke parameters and searched for evidence of extra solar CMEs.

4.5 Determining the Age of Nearby Young Neutron Stars

The final project of the thesis aims to determine the age of young nearby Neutron Stars (NS) using archival data from X-ray observatories such as *Chandra* and *XMM Newton*. Young NS have temperatures on the order of 10^6 K, which cool quite rapidly within the first 10^6 yrs. By measuring the blackbody emission from a neutron star, cooling rate can be determined, thus enabling the estimation of its age. At higher frequencies, observations are essentially blind to DM, making them indistinguishable at even appreciable differences (i.e., 0 – 40 pc/cc). By pairing measurements with LOFAR, which can determine DM on the scale of 10^{-3} pc/cc. Models of pulsar evolution can be tested once accurate measurements for P, $\dot{P}$, and age have been obtained.

5 Conclusion

This report outlines several projects, in section 1 and section 2 the theory of redback pulsars and how to search for them were discussed respectively. Unique for their close binary systems, low mass companion and transitional stages they provide a good tool for probing physical parameters of neutron stars. Observations of two *Fermi* redback candidates J0523 and J2054 have been carried out with Parkes and LOFAR respectively. A pipeline has been developed and employed on back-ends connected to each telescope and has successfully detected known pulsars. Further exploration of flag candidates is on going to determine a detection or non-detection of each candidate as described in section 2.3.5.

Additionally, the report describes the theory and methods of the first low-frequency SETI survey in section 1.5.2 and section 3. The survey encompasses target selection and the search for technosignatures among 1,631,152 targets, providing tight constraints on their prevalence in the Milky Way. The sensitivity to targets across their observed band and their emergence rate are illustrated in fig. 3.3 and fig. 3.4, respectively. Furthermore, outlines for a similar survey with NenuFAR observing *Kepler* and *TESS* targets are discussed, along with plans for a year-long Northern Hemispheric survey with LOFAR to search for both natural and unnatural transients using three stations.

Brief mention is made of ongoing work to explore the feasibility of detecting radio stars and exoplanets using a single LOFAR station. The motivation behind detecting radio emissions from these sources is discussed, along with plans to expand these observations in the coming months. Reliable detection of these sources and application to archival data could reveal new radio-loud M-dwarfs and potentially enable longer observations to detect emissions from ultra-cool dwarfs.

Finally, the last project of the PhD is outlined as an X-Ray project aiming to determine the ages of young neutron stars to better constrain models of neutron star evolution, a challenging and pressing question in the community. Full exploration of both the theory and methodology of this project will be undertaken upon completion of the three aforementioned projects.

References

Archibald, A. M., Stairs, I. H., Ransom, S. M., Kaspi, V. M., Kondratiev, V. I., Lorimer, D. R., McLaughlin, M. A., Boyles, J., Hessels, J. W. T., Lynch, R., van Leeuwen, J., Roberts, M. S. E., Jenet, F., Champion, D. J., Rosen, R., Barlow, B. N., Dunlap, B. H., and Remillard, R. A. (2009). A Radio Pulsar/X-ray Binary Link. *Science*, 324(5933):1411–1414. Publisher: American Association for the Advancement of Science.

ASTRON (2023). Lofar2.0 white paper - v2023.1.

Baym, G., Bethe, H. A., and Pethick, C. J. (1971). Neutron star matter. *Nuclear Physics A*, 175(2):225–271.

Borucki, W. J., Koch, D., Basri, G., Batalha, N., Brown, T., Caldwell, D., Caldwell, J., Christensen-Dalsgaard, J., Cochran, W. D., DeVore, E., Dunham, E. W., Dupree, A. K., Gautier, T. N., Geary, J. C., Gilliland, R., Gould, A., Howell, S. B., Jenkins, J. M., Kondo, Y., Latham, D. W., Marcy, G. W., Meibom, S., Kjeldsen, H., Lissauer, J. J., Monet, D. G., Morrison, D., Sasselov, D., Tarter, J., Boss, A., Brownlee, D., Owen, T., Buzasi, D., Charbonneau, D., Doyle, L., Fortney, J., Ford, E. B., Holman, M. J., Seager, S., Steffen, J. H., Welsh, W. F., Rowe, J., Anderson, H., Buchhave, L., Ciardi, D., Walkowicz, L., Sherry, W., Horch, E., Isaacson, H., Everett, M. E., Fischer, D., Torres, G., Johnson, J. A., Endl, M., MacQueen, P., Bryson, S. T., Dotson, J., Haas, M., Kolodziejczak, J., Van Cleve, J., Chandrasekaran, H., Twicken, J. D., Quintana, E. V., Clarke, B. D., Allen, C., Li, J., Wu, H., Tenenbaum, P., Verner, E., Bruhweiler, F., Barnes, J., and Prsa, A. (2010). Kepler Planet-Detection Mission: Introduction and First Results. *Science*, 327(5):977–.

Breton, R. P., Kerkwijk, M. H. v., Roberts, M. S. E., Hessels, J. W. T., Camilo, F., McLaughlin, M. A., Ransom, S. M., Ray, P. S., and Stairs, I. H. (2013). DISCOVERY OF THE OPTICAL COUNTERPARTS TO FOUR ENERGETIC FERMI MILLISECOND PULSARS. *The Astrophysical Journal*, 769(2):108. Publisher: The American Astronomical Society.

Callingham, J. R., Pope, B. J. S., Kavanagh, R. D., Bellotti, S., Daley-Yates, S., Damasso, M., Grießmeier, J.-M., Güdel, M., Günther, M., Kao, M. M., Klein, B., Mahadevan, S., Morin, J., Nichols, J. D., Osten, R. A., Pérez-Torres, M., Pineda, J. S., Rigney, J., Saur, J., Stefánsson, G., Turner, J., Vedantham, H., Vidotto, A. A., Villadsen, J., and Zarka, P. (2024). Radio stars and exoplanets. *Nature Astronomy*.

Chandrasekhar, S. (1967). *An Introduction to the Study of Stellar Structure*. Dover Books on Astronomy Series. Dover Publications, Incorporated.

Clark, C. J., Kerr, M., Barr, E. D., Bhattacharyya, B., Breton, R. P., Bruel, P., Camilo, F., Chen, W., Cognard, I., Cromartie, H. T., Deneva, J., Dhillon, V. S., Guillemot, L., Kennedy, M. R., Kramer, M., Lyne, A. G., Sánchez, D. M., Nieder, L., Phillips, C., Ransom, S. M., Ray, P. S., Roberts, M. S. E., Roy, J., Smith, D. A., Spiewak, R., Stappers, B. W., Tabassum, S., Theureau, G., and Voisin, G. (2023). Neutron star mass estimates from gamma-ray eclipses in spider millisecond pulsar binaries. *Nature Astronomy*, 7(4):451–462. Publisher: Nature Publishing Group.

Corbet, R. H. D., Chomiuk, L., Coley, J. B., Dubus, G., Edwards, P. G., Islam, N., McBride, V. A., Stevens, J., Strader, J., Swihart, S. J., and Townsend, L. J. (2022). Gamma-Ray Eclipses and Orbital Modulation Transitions in the Candidate Redback 4FGL J1702.7–5655. *The Astrophysical Journal*, 935(1):2. Publisher: The American Astronomical Society.

Cordes, J. M. and Lazio, T. J. W. (2003). NE2001.I. A New Model for the Galactic Distribution of Free Electrons and its Fluctuations. arXiv:astro-ph/0207156.

Drake, F. D. (1961). Project Ozma. *Physics Today*, 14(4):40.

Enriquez, J. E., Siemion, A., Foster, G., Gajjar, V., Hellbourg, G., Hickish, J., Isaacson, H., Price, D. C., Croft, S., DeBoer, D., Lebofsky, M., MacMahon, D. H. E., and Werthimer, D. (2017). The Breakthrough Listen Search for Intelligent Life: 1.1-1.9 GHz Observations of 692 Nearby Stars. *The Astrophysical Journal*, 849:104.

Gaia Collaboration, Vallenari, A., Brown, A. G. A., Prusti, T., de Bruijne, J. H. J., Arenou, F., Babusiaux, C., Biermann, M., Creevey, O. L., Ducourant, C., Evans, D. W., Eyer, L., Guerra, R., Hutton, A., Jordi, C., Klioner, S. A., Lammers, U. L., Lindegren, L., Luri, X., Mignard, F., Panem, C., Pourbaix, D., Randich, S., Sartoretti, P., Soubiran, C., Tanga, P., Walton, N. A., Bailer-Jones, C. A. L., Bastian, U., Drimmel, R., Jansen, F., Katz, D., Lattanzi, M. G., van Leeuwen, F., Bakker, J., Cacciari, C., Castañeda, J., De Angeli, F., Fabricius, C., Fouesneau, M., Frémat, Y., Galluccio, L., Guerrier, A., Heiter, U., Masana, E., Messineo, R., Mowlavi, N., Nicolas, C., Nienartowicz, K., Pailler, F., Panuzzo, P., Riclet, F., Roux, W., Seabroke, G. M., Sordo, R., Thévenin, F., Gracia-Abril, G., Portell, J., Teyssier, D., Altmann, M., Andrae, R., Audard, M., Bellas-Velidis, I., Benson, K., Berthier, J., Blomme, R., Burgess, P. W., Busonero, D., Busso, G., Cánovas, H., Carry, B., Cellino, A., Cheek, N., Clementini, G., Damerdji, Y., Davidson, M., de Teodoro, P., Nuñez Campos, M., Delchambre, L., Dell'Oro, A., Esquej, P., Fernández-Hernández, J., Fraile, E., Garabato, D., García-Lario, P., Gosset, E., Haigron, R., Halbwachs, J. L., Hambly, N. C., Harrison, D. L., Hernández, J., Hestroffer, D., Hodgkin, S. T., Holl, B., Janßen, K., Jevardat de Fombelle, G., Jordan, S., Krone-Martins, A., Lanzafame, A. C., Löffler,

W., Marchal, O., Marrese, P. M., Moitinho, A., Muinonen, K., Osborne, P., Pancino, E., Pauwels, T., Recio-Blanco, A., Reylé, C., Riello, M., Rimoldini, L., Roegiers, T., Rybizki, J., Sarro, L. M., Siopis, C., Smith, M., Sozzetti, A., Utrilla, E., van Leeuwen, M., Abbas, U., Ábrahám, P., Abreu Aramburu, A., Aerts, C., Aguado, J. J., Ajaj, M., Aldea-Montero, F., Altavilla, G., Álvarez, M. A., Alves, J., Anders, F., Anderson, R. I., Anglada Varela, E., Antoja, T., Baines, D., Baker, S. G., Balaguer-Núñez, L., Balbinot, E., Balog, Z., Barache, C., Barbato, D., Barros, M., Barstow, M. A., Bartolomé, S., Bassilana, J. L., Bauchet, N., Becciani, U., Bellazzini, M., Berihuete, A., Bernet, M., Bertone, S., Bianchi, L., Binnenfeld, A., Blanco-Cuaresma, S., Blazere, A., Boch, T., Bombrun, A., Bossini, D., Bouquillon, S., Bragaglia, A., Bramante, L., Breedt, E., Bressan, A., Brouillet, N., Brugaletta, E., Bucciarelli, B., Burlacu, A., Butkevich, A. G., Buzzi, R., Caffau, E., Cancelliere, R., Cantat-Gaudin, T., Carballo, R., Carlucci, T., Carnerero, M. I., Carrasco, J. M., Casamiquela, L., Castellani, M., Castro-Ginard, A., Chaoul, L., Charlot, P., Chemin, L., Chiaramida, V., Chiavassa, A., Chornay, N., Comoretto, G., Contursi, G., Cooper, W. J., Cornez, T., Cowell, S., Crifo, F., Cropper, M., Crosta, M., Crowley, C., Dafonte, C., Dapergolas, A., David, M., David, P., de Laverny, P., De Luise, F., De March, R., De Ridder, J., de Souza, R., de Torres, A., del Peloso, E. F., del Pozo, E., Delbo, M., Delgado, A., Delisle, J. B., Demouchy, C., Dharmawardena, T. E., Di Matteo, P., Diakite, S., Diener, C., Distefano, E., Dolding, C., Edvardsson, B., Enke, H., Fabre, C., Fabrizio, M., Faigler, S., Fedorets, G., Fernique, P., Fienga, A., Figueras, F., Fournier, Y., Fouron, C., Fragkoudi, F., Gai, M., Garcia-Gutierrez, A., Garcia-Reinaldos, M., García-Torres, M., Garofalo, A., Gavel, A., Gavras, P., Gerlach, E., Geyer, R., Giacobbe, P., Gilmore, G., Girona, S., Giuffrida, G., Gomel, R., Gomez, A., González-Núñez, J., González-Santamaría, I., González-Vidal, J. J., Granvik, M., Guillout, P., Guiraud, J., Gutiérrez-Sánchez, R., Guy, L. P., Hatzidimitriou, D., Hauser, M., Haywood, M., Helmer, A., Helmi, A., Sarmiento, M. H., Hidalgo, S. L., Hilger, T., Hładczuk, N., Hobbs, D., Holland, G., Huckle, H. E., Jardine, K., Jasniewicz, G., Jean-Antoine Piccolo, A., Jiménez-Arranz, Ó., Jorissen, A., Juaristi Campillo, J., Julbe, F., Karbevska, L., Kervella, P., Khanna, S., Kontizas, M., Kordopatis, G., Korn, A. J., Kóspál, Á., Kostrzewa-Rutkowska, Z., Kruszyńska, K., Kun, M., Laizeau, P., Lambert, S., Lanza, A. F., Lasne, Y., Le Campion, J. F., Lebreton, Y., Lebzelter, T., Leccia, S., Leclerc, N., Lecoeur-Taibi, I., Liao, S., Licata, E. L., Lindstrøm, H. E. P., Lister, T. A., Livanou, E., Lobel, A., Lorca, A., Loup, C., Madrero Pardo, P., Magdaleno Romeo, A., Managau, S., Mann, R. G., Manteiga, M., Marchant, J. M., Marconi, M., Marcos, J., Marcos Santos, M. M. S., Marín Pina, D., Marinoni, S., Marocco, F., Marshall, D. J., Martin Polo, L., Martín-Fleitas, J. M., Marton, G., Mary, N., Masip, A., Massari, D., Mastrobuono-Battisti, A., Mazeh, T., McMillan, P. J., Messina, S., Michalik, D., Millar, N. R., Mints, A., Molina, D., Molinaro, R., Molnár, L., Monari, G., Monguió, M., Montegriffo, P., Mon-

tero, A., Mor, R., Mora, A., Morbidelli, R., Morel, T., Morris, D., Muraveva, T., Murphy, C. P., Musella, I., Nagy, Z., Noval, L., Ocaña, F., Ogden, A., Ordenovic, C., Osinde, J. O., Pagani, C., Pagano, I., Palaversa, L., Palicio, P. A., Pallas-Quintela, L., Panahi, A., Payne-Wardenaar, S., Peñalosa Esteller, X., Penttilä, A., Pichon, B., Piersimoni, A. M., Pineau, F. X., Plachy, E., Plum, G., Poggio, E., Prša, A., Pulone, L., Racero, E., Ragaini, S., Rainer, M., Raiteri, C. M., Rambaux, N., Ramos, P., Ramos-Lerate, M., Re Fiorentin, P., Regibo, S., Richards, P. J., Rios Diaz, C., Ripepi, V., Riva, A., Rix, H. W., Rixon, G., Robichon, N., Robin, A. C., Robin, C., Roelens, M., Rogues, H. R. O., Rohrbasser, L., Romero-Gómez, M., Rowell, N., Royer, F., Ruz Mieres, D., Rybicki, K. A., Sadowski, G., Sáez Núñez, A., Sagristà Sellés, A., Sahlmann, J., Salguero, E., Samaras, N., Sanchez Gimenez, V., Sanna, N., Santoveña, R., Sarasso, M., Schultheis, M., Sciacca, E., Segol, M., Segovia, J. C., Ségransan, D., Semeux, D., Shahaf, S., Siddiqui, H. I., Siebert, A., Siltala, L., Silvelo, A., Slezak, E., Slezak, I., Smart, R. L., Snaith, O. N., Solano, E., Solitro, F., Souami, D., Souchay, J., Spagna, A., Spina, L., Spoto, F., Steele, I. A., Steidelmüller, H., Stephenson, C. A., Süveges, M., Surdej, J., Szabados, L., Szegedi-Elek, E., Taris, F., Taylor, M. B., Teixeira, R., Tolomei, L., Tonello, N., Torra, F., Torra, J., Torralba Elipe, G., Trabucchi, M., Tsounis, A. T., Turon, C., Ulla, A., Unger, N., Vaillant, M. V., van Dillen, E., van Reeven, W., Vanel, O., Vecchiato, A., Viala, Y., Vicente, D., Voutsinas, S., Weiler, M., Wevers, T., Wyrzykowski, Ł., Yoldas, A., Yvard, P., Zhao, H., Zorec, J., Zucker, S., and Zwitter, T. (2023). Gaia Data Release 3. Summary of the content and survey properties. *aap*, 674:A1.

Gajjar, V., LeDuc, D., Chen, J., Siemion, A. P. V., Sheikh, S. Z., Brzycki, B., Croft, S., Czech, D., DeBoer, D., DeMarines, J., Drew, J., Isaacson, H., Lacki, B. C., Lebofsky, M., MacMahon, D. H. E., Ng, C., de Pater, I., Perez, K. I., Price, D. C., Suresh, A., Webb, C., and Worden, S. P. (2022). Searching for Broadband Pulsed Beacons from 1883 Stars Using Neural Networks. *ApJ*, 932(2):81.

Gehrels, N. (1986). Confidence Limits for Small Numbers of Events in Astrophysical Data. *ApJ*, 303:336.

Ginsburg, A., Sipőcz, B. M., Brasseur, C. E., Cowperthwaite, P. S., Craig, M. W., Deil, C., Guillochon, J., Guzman, G., Liedtke, S., Lian Lim, P., Lockhart, K. E., Mommert, M., Morris, B. M., Norman, H., Parikh, M., Persson, M. V., Robitaille, T. P., Segovia, J.-C., Singer, L. P., Tollerud, E. J., de Val-Borro, M., Valtchanov, I., Woillez, J., The Astroquery collaboration, and a subset of the astropy collaboration (2019). astroquery: An Astronomical Web-querying Package in Python. *The Astronomical Journal*, 157:98.

Hallinan, G., Antonova, A., Doyle, J. G., Bourke, S., Brisken, W. F., and Golden, A. (2006). Rotational Modulation of the Radio Emission from the M9 Dwarf TVLM

513–46546: Broadband Coherent Emission at the Substellar Boundary? *The Astrophysical Journal*, 653(1):690. Publisher: IOP Publishing.

Halpern, J. P., Perez, K. I., and Bogdanov, S. (2022). Luminous Optical and X-ray Flaring of the Putative Redback Millisecond Pulsar 1FGL J0523.5$-$2529. *The Astrophysical Journal*, 935(2):151. arXiv:2207.08198 [astro-ph].

Hankins, T. H. and Rickett, B. J. (1975). Pulsar signal processing. *Methods in Computational Physics*, 14:55–129. ADS Bibcode: 1975MComP..14...55H.

Heger, A., Fryer, C. L., Woosley, S. E., Langer, N., and Hartmann, D. H. (2003). How Massive Single Stars End Their Life. *The Astrophysical Journal*, 591:288–300. ADS Bibcode: 2003ApJ...591..288H.

Hewish, A., Bell, S. J., Pilkington, J. D. H., Scott, P. F., and Collins, R. A. (1968). Observation of a Rapidly Pulsating Radio Source. *Nature*, 217(5130):709–713.

Johnson, O. A., Gajjar, V., Keane, E. F., McKenna, D. J., Giese, C., McKeon, B., Carozzi, T. D., Alcaria, C., Brennan, A., Brzycki, B., Croft, S., Drew, J., Elkins, R., Gallagher, P. T., Kelly, R., Lebofsky, M., MacMahon, D. H. E., McCauley, J., Pater, I. d., Raeside, S. R., Siemion, A. P. V., and Worden, S. P. (2023). A Simultaneous Dual-site Technosignature Search Using International LOFAR Stations. *The Astronomical Journal*, 166(5):193. Publisher: The American Astronomical Society.

Karpova, A. V., Zyuzin, D. A., Shibanov, Y. A., and Gilfanov, M. R. (2023). A new redback pulsar candidate 4FGL J2054.2+6904. *Monthly Notices of the Royal Astronomical Society*, 524(2):3020–3025. arXiv:2306.17593 [astro-ph].

Kaspi, V. M., Roberts, M. E., Vasisht, G., Gotthelf, E. V., Pivovaroff, M., and Kawai, N. (2001). Chandra X-Ray Observations of G11.2-0.3: Implications for Pulsar Ages. *The Astrophysical Journal*, 560:371–377. ADS Bibcode: 2001ApJ...560..371K.

Kasting, J. F., Whitmire, D. P., and Reynolds, R. T. (1993). Habitable Zones around Main Sequence Stars. *Icarus*, 101(1):108–128.

Kavanagh, R. D. and Vedantham, H. K. (2023). Hunting for exoplanets via magnetic star–planet interactions: geometrical considerations for radio emission. *Monthly Notices of the Royal Astronomical Society*, 524(4):6267–6284.

Kumar, P. and Western, A. (2021). How can the fourier transform be used in radio astronomy to perform spectral analysis of pulsars. *Journal of Student Research*, 10.

Lattimer, J. M. and Prakash, M. (2001). Neutron Star Structure and the Equation of State. *The Astrophysical Journal*, 550(1):426.

Lebofsky, M., Croft, S., Siemion, A. P. V., Price, D. C., Enriquez, J. E., Isaacson, H., MacMahon, D. H. E., Anderson, D., Brzycki, B., Cobb, J., Czech, D., DeBoer, D., DeMarines, J., Drew, J., Foster, G., Gajjar, V., Gizani, N., Hellbourg, G., Korpela, E. J., Lacki, B., Sheikh, S., Werthimer, D., Worden, P., Yu, A., and Zhang, Y. G. (2019). The Breakthrough Listen Search for Intelligent Life: Public Data, Formats, Reduction, and Archiving. *PASP*, 131(1006):124505.

Li, J.-K., Zhao, H.-C., Tao, Z.-Z., Zhang, T.-J., and Xiao-Hui, S. (2022). Drift Rates of Narrowband Signals in Long-term SETI Observations for Exoplanets. *The Astrophysical Journal*, 938(1):1.

Lorimer, D. R. and Kramer, M. (2004). *Handbook of Pulsar Astronomy*, volume 4. Cambridge University Press.

Lynch, C., Murphy, T., Ravi, V., Hobbs, G., Lo, K., and Ward, C. (2016). Radio detections of southern ultracool dwarfs. *Monthly Notices of the Royal Astronomical Society*, 457(2):1224–1232.

Martini, P., Stoll, R., Derwent, M. A., Zhelem, R., Atwood, B., Gonzalez, R., Mason, J. A., O'Brien, T. P., Pappalardo, D. P., Pogge, R. W., Ward, B., and Wong, M.-H. (2011). The Ohio State Multi-Object Spectrograph. *Publications of the Astronomical Society of the Pacific*, 123(900):187. Publisher: University of Chicago Press.

McKenna, D. J., Keane, E. F., Gallagher, P. T., and McAuley, J. (2023). udpPacketManager: An International LOFAR Station Data (Pre-)Processor. *The Journal of Open Source Software*.

Michel, F. C. (1982). Theory of pulsar magnetospheres. *Reviews of Modern Physics*, 54(1):1–66. Publisher: American Physical Society.

Murphy, P. C., Carley, E. P., Ryan, A. M., Zucca, P., and Gallagher, P. T. (2021). LOFAR observations of radio burst source sizes and scattering in the solar corona. *Astronomy and Astrophysics*, 645:A11. ADS Bibcode: 2021A&A...645A..11M.

Ng, C., Champion, D. J., Bailes, M., Barr, E. D., Bates, S. D., Bhat, N. D. R., Burgay, M., Burke-Spolaor, S., Flynn, C. M. L., Jameson, A., Johnston, S., Keith, M. J., Kramer, M., Levin, L., Petroff, E., Possenti, A., Stappers, B. W., van Straten, W., Tiburzi, C., Eatough, R. P., and Lyne, A. G. (2015). The High Time Resolution Universe Pulsar Survey – XII. Galactic plane acceleration search and the discovery of 60 pulsars. *Monthly Notices of the Royal Astronomical Society*, 450(3):2922–2947.

Ng, C., Rizk, L., Mannion, C., and Keane, E. F. (2022). Search for Extraterrestrial Intelligence with the ngVLA. *The Astronomical Journal*, 164:205. ADS Bibcode: 2022AJ....164..205N.

Oppenheimer, J. R. and Volkoff, G. M. (1939). On Massive Neutron Cores. *Physical Review*, 55(4):374–381. Publisher: American Physical Society.

Papitto, A. and de Martino, D. (2022). Transitional Millisecond Pulsars. 465:157–200. Conference Name: Astrophysics and Space Science Library Place: eprint: arXiv:2010.09060 ADS Bibcode: 2022ASSL..465..157P.

Ransom, S. M. (2001). *New search techniques for binary pulsars*. PhD thesis. Publication Title: Ph.D. Thesis ADS Bibcode: 2001PhDT.....123R.

Ray, P. S., Abdo, A. A., Parent, D., Bhattacharya, D., Bhattacharyya, B., Camilo, F., Cognard, I., Theureau, G., Ferrara, E. C., Harding, A. K., Thompson, D. J., Freire, P. C. C., Guillemot, L., Gupta, Y., Roy, J., Hessels, J. W. T., Johnston, S., Keith, M., Shannon, R., Kerr, M., Michelson, P. F., Romani, R. W., Kramer, M., McLaughlin, M. A., Ransom, S. M., Roberts, M. S. E., Parkinson, P. M. S., Ziegler, M., Smith, D. A., Stappers, B. W., Weltevrede, P., and Wood, K. S. (2012). Radio Searches of Fermi LAT Sources and Blind Search Pulsars: The Fermi Pulsar Search Consortium. arXiv:1205.3089 [astro-ph].

Ricker, G. R., Winn, J. N., Vanderspek, R., Latham, D. W., Bakos, G. Á., Bean, J. L., Berta-Thompson, Z. K., Brown, T. M., Buchhave, L., Butler, N. R., Butler, R. P., Chaplin, W. J., Charbonneau, D., Christensen-Dalsgaard, J., Clampin, M., Deming, D., Doty, J., De Lee, N., Dressing, C., Dunham, E. W., Endl, M., Fressin, F., Ge, J., Henning, T., Holman, M. J., Howard, A. W., Ida, S., Jenkins, J. M., Jernigan, G., Johnson, J. A., Kaltenegger, L., Kawai, N., Kjeldsen, H., Laughlin, G., Levine, A. M., Lin, D., Lissauer, J. J., MacQueen, P., Marcy, G., McCullough, P. R., Morton, T. D., Narita, N., Paegert, M., Palle, E., Pepe, F., Pepper, J., Quirrenbach, A., Rinehart, S. A., Sasselov, D., Sato, B., Seager, S., Sozzetti, A., Stassun, K. G., Sullivan, P., Szentgyorgyi, A., Torres, G., Udry, S., and Villasenor, J. (2015). Transiting Exoplanet Survey Satellite (TESS). *Journal of Astronomical Telescopes, Instruments, and Systems*, 1:014003.

Roberts, M. S. E., Noori, H. A., Torres, R. A., McLaughlin, M. A., Gentile, P. A., Hessels, J. W. T., Ransom, S. M., Ray, P. S., Kerr, M., and Breton, R. P. (2017). X-Ray and Optical Properties of Black Widows and Redbacks. *Proceedings of the International Astronomical Union*, 13(S337):43–46.

Romani, R. W., Kandel, D., Filippenko, A. V., Brink, T. G., and Zheng, W. (2022). Psr j0952-0607: The fastest and heaviest known galactic neutron star. *The Astrophysical Journal Letters*, 934(2):L17.

Shapiro, S. L. and Teukolsky, S. A. (1983). *Black holes, white dwarfs and neutron stars. The physics of compact objects*.

Sheikh, S. Z. (2020). Nine axes of merit for technosignature searches. *International Journal of Astrobiology*, 19(3):237–243.

Sheikh, S. Z., Wright, J. T., Siemion, A., and Enriquez, J. E. (2019). Choosing a maximum drift rate in a seti search: Astrophysical considerations. *The Astrophysical Journal*, 884(1):14.

Shklovskii, I. S. and Sagan, C. (1966). *Intelligent life in the universe*.

Siemion, A. P. V., Demorest, P., Korpela, E., Maddalena, R. J., Werthimer, D., Cobb, J., Howard, A. W., Langston, G., Lebofsky, M., Marcy, G. W., and Tarter, J. (2013). A 1.1-1.9 GHz SETI Survey of the Kepler Field. I. A Search for Narrow-band Emission from Select Targets. *The Astrophysical Journal*, 767:94.

Strader, J., Chomiuk, L., Sonbas, E., Sokolovsky, K., Sand, D. J., Moskvitin, A. S., and Cheung, C. C. (2014). 1FGL J0523.5-2529: A New Probable Gamma-ray Pulsar Binary. *The Astrophysical Journal*, 788(2):L27. arXiv:1405.5533 [astro-ph].

Strader, J., Swihart, S., Chomiuk, L., Bahramian, A., Britt, C., Cheung, C. C., Dage, K., Halpern, J., Li, K.-L., Mignani, R. P., Orosz, J. A., Peacock, M., Salinas, R., Shishkovsky, L., and Tremou, E. (2019). Optical Spectroscopy and Demographics of Redback Millisecond Pulsar Binaries. *The Astrophysical Journal*, 872(1):42. Publisher: The American Astronomical Society.

Takata, J., Li, K. L., Leung, G. C. K., Kong, A. K. H., Tam, P. H. T., Hui, C. Y., Wu, E. M. H., Xing, Y., Cao, Y., Tang, S., Wang, Z., and Cheng, K. S. (2014). Multi-wavelength emissions from the millisecond pulsar binary psr j1023+0038 during an accretion active state. *The Astrophysical Journal*, 785(2):131. Publisher: The American Astronomical Society.

Tarter, J. C. (1996). Project Phoenix: the Australian deployment. In Kingsley, S. A. and Lemarchand, G. A., editors, *Photonics West '96*, pages 24–34. SPIE.

Taylor, J. H. and Manchester, R. N. (1977). Recent observations of pulsars. *Annual Review of Astronomy and Astrophysics*, 15:19–44. ADS Bibcode: 1977ARA&A..15...19T.

van Haarlem, M. P., Wise, M. W., Gunst, A. W., Heald, G., McKean, J. P., Hessels, J. W. T., de Bruyn, A. G., Nijboer, R., Swinbank, J., Fallows, R., Brentjens, M., Nelles, A., Beck, R., Falcke, H., Fender, R., Hörandel, J., Koopmans, L. V. E., Mann, G., Miley, G., Röttgering, H., Stappers, B. W., Wijers, R. a. M. J., Zaroubi, S., van den Akker, M., Alexov, A., Anderson, J., Anderson, K., van Ardenne, A., Arts, M., Asgekar, A., Avruch, I. M., Batejat, F., Bähren, L., Bell, M. E., Bell, M. R., van Bemmel,

I., Bennema, P., Bentum, M. J., Bernardi, G., Best, P., Bîrzan, L., Bonafede, A., Boonstra, A.-J., Braun, R., Bregman, J., Breitling, F., van de Brink, R. H., Broderick, J., Broekema, P. C., Brouw, W. N., Brüggen, M., Butcher, H. R., van Cappellen, W., Ciardi, B., Coenen, T., Conway, J., Coolen, A., Corstanje, A., Damstra, S., Davies, O., Deller, A. T., Dettmar, R.-J., van Diepen, G., Dijkstra, K., Donker, P., Doorduin, A., Dromer, J., Drost, M., van Duin, A., Eislöffel, J., van Enst, J., Ferrari, C., Frieswijk, W., Gankema, H., Garrett, M. A., de Gasperin, F., Gerbers, M., de Geus, E., Grießmeier, J.-M., Grit, T., Gruppen, P., Hamaker, J. P., Hassall, T., Hoeft, M., Holties, H. A., Horneffer, A., van der Horst, A., van Houwelingen, A., Huijgen, A., Iacobelli, M., Intema, H., Jackson, N., Jelic, V., de Jong, A., Juette, E., Kant, D., Karastergiou, A., Koers, A., Kollen, H., Kondratiev, V. I., Kooistra, E., Koopman, Y., Koster, A., Kuniyoshi, M., Kramer, M., Kuper, G., Lambropoulos, P., Law, C., van Leeuwen, J., Lemaitre, J., Loose, M., Maat, P., Macario, G., Markoff, S., Masters, J., McFadden, R. A., McKay-Bukowski, D., Meijering, H., Meulman, H., Mevius, M., Middelberg, E., Millenaar, R., Miller-Jones, J. C. A., Mohan, R. N., Mol, J. D., Morawietz, J., Morganti, R., Mulcahy, D. D., Mulder, E., Munk, H., Nieuwenhuis, L., van Nieuwpoort, R., Noordam, J. E., Norden, M., Noutsos, A., Offringa, A. R., Olofsson, H., Omar, A., Orrú, E., Overeem, R., Paas, H., Pandey-Pommier, M., Pandey, V. N., Pizzo, R., Polatidis, A., Rafferty, D., Rawlings, S., Reich, W., de Reijer, J.-P., Reitsma, J., Renting, G. A., Riemers, P., Rol, E., Romein, J. W., Roosjen, J., Ruiter, M., Scaife, A., van der Schaaf, K., Scheers, B., Schellart, P., Schoenmakers, A., Schoonderbeek, G., Serylak, M., Shulevski, A., Sluman, J., Smirnov, O., Sobey, C., Spreeuw, H., Steinmetz, M., Sterks, C. G. M., Stiepel, H.-J., Stuurwold, K., Tagger, M., Tang, Y., Tasse, C., Thomas, I., Thoudam, S., Toribio, M. C., van der Tol, B., Usov, O., van Veelen, M., van der Veen, A.-J., ter Veen, S., Verbiest, J. P. W., Vermeulen, R., Vermaas, N., Vocks, C., Vogt, C., de Vos, M., van der Wal, E., van Weeren, R., Weggemans, H., Weltevrede, P., White, S., Wijnholds, S. J., Wilhelmsson, T., Wucknitz, O., Yatawatta, S., Zarka, P., Zensus, A., and van Zwieten, J. (2013). LOFAR: The LOw-Frequency ARray. *Astronomy & Astrophysics, Volume 556, id.A2, <NUMPAGES>53</NUMPAGES> pp.*, 556:A2.

Vedantham, H. K., Callingham, J. R., Shimwell, T. W., Tasse, C., Pope, B. J. S., Bedell, M., Snellen, I., Best, P., Hardcastle, M. J., Haverkorn, M., Mechev, A., O'Sullivan, S. P., Röttgering, H. J. A., and White, G. J. (2020). Coherent radio emission from a quiescent red dwarf indicative of star-planet interaction. *Nature Astronomy*, 4:577–583. ADS Bibcode: 2020NatAs...4..577V.

Villadsen, J. and Hallinan, G. (2019). Ultra-wideband Detection of 22 Coherent Radio Bursts on M Dwarfs. *The Astrophysical Journal*, 871(2):214. Publisher: The American Astronomical Society.

Wlodarczyk-Sroka, B. S., Garrett, M. A., and Siemion, A. P. V. (2020). Extending the Breakthrough Listen nearby star survey to other stellar objects in the field. *MNRAS*, 498(4):5720–5729.

Yao, J. M., Manchester, R. N., and Wang, N. (2017). A NEW ELECTRON-DENSITY MODEL FOR ESTIMATION OF PULSAR AND FRB DISTANCES. *The Astrophysical Journal*, 835(1):29. Publisher: The American Astronomical Society.

Zarka, P. (1998). Auroral radio emissions at the outer planets: Observations and theories. *Journal of Geophysical Research: Planets*, 103(E9):20159–20194. _eprint: https://onlinelibrary.wiley.com/doi/pdf/10.1029/98JE01323.

Zhelezniakov, V. V. and Zlotnik, E. I. (1975). Cyclotron Wave Instability in the Corona and Origin of Solar Radio Emission with Fine Structure. I: Bernstein Modes and Plasma Waves in a Hybrid Band. 43(2):431–451.